FRACTURE ANALYSIS OF THE BOLSHOI KARATAU UPPER PALEOZOIC CARBONATE PLATFORM AS A WELL-EXPOSED ANALOG TO THE TENGIZ FRACTURED CARBONATE PETROLEUM-RESERVOIR

by

DIAS BEKESHOV

THESIS SUPERVISOR

SEBASTIANUS WILLEM JOSEF DEN BROK

THESIS CO-SUPERVISOR

RANDY HAZLETT

Thesis submitted to the School of Mining and Geosciences of Nazarbayev University in Partial Fulfillment of the Requirements for the Degree of **Master of Science in Petroleum Engineering**

Nazarbayev University
15.04.2025

ORIGINALITY STATEMENT

I, Dias Bekeshov, hereby declare that this submission is my own work and to the best of my knowledge it contains no materials previously published or written by another person, or substantial proportions of material which have been accepted for the award of any other degree or diploma at Nazarbayev University or any other educational institution, except where due acknowledgement is made in the thesis.

Any contribution made to the research by others, with whom I have worked at NU or elsewhere is explicitly acknowledged in the thesis.

I also declare that the intellectual content of this thesis is the product of my own work, except to the extent that assistance from others in the project's design and conception or in style, presentation and linguistic expression is acknowledged.

Signed on 15.04.2025

ABSTRACT

The Tengiz oilfield in western Kazakhstan is one of the major oilfields in Kazakhstan. It is a fractured carbonate reservoir, a lower Paleozoic carbonate platform. TengizChevrOil is presently investigating the fracture properties of the outer carbonate platform slope of the reservoir. As rocks at Tengiz are not exposed and only accessible through drilling, fracture properties were studied in the well-exposed carbonate platform in the Bolshoi Karatau mountains which is regarded as an analogue platform.

The carbonate platform in the Bolshoi Karatau mountains are of the same age and similar lithology as in the Tengiz platform. It is well exposed, because the platform was uplifted to form a mountain range during Hercynian and Alpine deformation phases. The outboard lower slope of the Bolshoi Karatau platform is represented by the Baktysai Formation, in which open fractures had turned into completely mineralized fractures, i.e. calcite veins. These were analyzed in grainstones and rudstones in three key outcrop locations: Aktobe, Akuyuk and Zhankorgan sections.

Scanline measurements of 6.0 ± 2.0 m long were collected to characterize the veins, while collecting orientations and vein dimensions (kinematic aperture, length, height). From this data set, spacing was derived. In addition, Schmidt hammer measurements were collected to determine Youngs Modulus of the various rock types that host the veins. It should be noted that the vein width is aperture and since they are fully filled, we also might refer as "kinematic aperture". In the Aktobe section, the dominant vein set has an average width of 3.7 ± 1.0 mm, an average spacing of 0.2 ± 0.1 m, an average height of 0.3 ± 0.1 m and occur in beds of 1.0 ± 0.5 m thick. In the Akuyuk section the dominant vein set has an average vein width of 1.0 ± 0.6 mm, with an average spacing of 0.1 ± 0.02 m and an average height of 0.3 ± 0.1 m in beds of 0.2 ± 0.1 m thick.

No significant correlation was found between bed thickness and either vein intensity or vein spacing, with R^2 values of 0.11 and 0.21 for grainstone and rudstone, respectively. Similarly, Dunham classification and facies types did not show a strong relationship with vein characteristics. The calcite vein coverage, expressed as a percentage of the wall rock for the dominant set is 2.0 ± 0.7 % in the Aktobe section and 0.4 ± 0.1 % in the Akuyuk section. Young's modulus of the grainstones and the rudstones derived from Schmidt hammer rebound values is 66 ± 12 Gpa, with slight difference between the two rocktypes

It was concluded on the based on theoretical calculations of the maximum vein width and relative age relations that the calcite veins in the Baktysai Formation are not burial veins (i.e. did not form due to the burial nor during the burial), but formed as 'tectonic' veins during the Hercynian mountain building. It further appeared that the presence of Hercynian faults near the sections exerts a significant role on the vein statistics as does the presence of stylolites that developed before and after the veins. Vein width of dominant sets was plotted in cummulative log-log plot. Both sections exhibit multi segmented power-law behavior, with segmented trendlines. The slope of linear parts of the curves falls in the range of –0.43 to –2.03 in the Aktobe section, while Akuyuk section shows slopes of –0.11 and –0.91. Nonlinearity of the curves was shown to be possibly due to insufficient length of the scanlines. The results suggest that, ideally, they should be longer than 10 m to avoid abnormalities caused by variations in local stress conditions.

ACKNOWLEDGMENT

I extend my deepest gratitude to my supervisor, Professor Sebastianus Willem Josef Den Brok, whose expertise and guidance made this research possible. I am sincerely thankful for the extensive knowledge I gained during two years of Master's program, as well as for his patience and unwavering support throughout this journey. Professor Den Brok is a true scientist with a deep passion for geology, and he made a remarkable effort to share the beauty of structural geology with me, a student pursuing a Master's in Petroleum Engineering and holding a Bachelor's degree in Chemical and Materials Engineering. Professor Den Brok never once doubted me, instead, he always believed in me. He has been not only an exceptional academic advisor, but also a life mentor and a trusted friend.

I would also like to extend my heartfelt thanks to my co-supervisor, Professor Randy Hazlett, for his continuous support and mentorship throughout the Master's program.

In addition, I am sincerely grateful to Chevron for providing the financial support that was essential not only for the successful completion of this research but also for sponsoring my Master's studies.

I would like to give special acknowledgment to Professor Arnoud Slootman, Professor Zane Job and Dr. James Bishop for their guidance and support of NU students. Their expertise in carbonate sedimentology, particularly during fieldwork, was invaluable to this research.

Last but least, I would like to thank Dinara Nadirkhanova, Togzhan Mynbayeva, Amir Umralin, Alisher Igizgali, Rachel Williams, Marat Ibagarov, Guldana Alimzhanova and Sanzhar Begimbetov for assisting in data collection.

TABLE OF CONTENTS

LIST OF FIGURES

LIST OF TABLES

1. INTRODUCTION

1.1. Background/Problem Definition

Tengiz is one of the giant onshore and offshore hydrocarbons bearing Paleozoic carbonate reservoirs located in the Primorsk Archipelago, Kazakhstan (**Figure 1a**). It is characterized as an isolated, steep-sided carbonate platform in the Precaspian Basin, where carboniferous platform and slope facies play as a source of hydrocarbon extraction (Collins et al., 2013, 2006; Weber et al., 2003). It was estimated that Tengiz holds about 3.1 billion tons of oil in place, where recoverable crude oil is about 1.2 billion tons (Tengizchevroil, 2023). Tengiz currently is experiencing pressure decline in the upper slope and rim, where most of the production has occurred. The lower slope where gravity flow deposits are observed, is generally at higher pressures due to less depletion, but relatively less characterized (**Figure 1b**). Previous works have characterized complexities of fracture networks and recovery mechanisms in the field, utilizing mainly data collected from wellbore image logs. Although, image logs might offer information regarding the fracture width and intensity, data about fracture height or length, their terminations and relation with bed thicknesses, facies and stylolites cannot be obtained. Therefore, other methods such as analogue studies are needed to supplement required information.

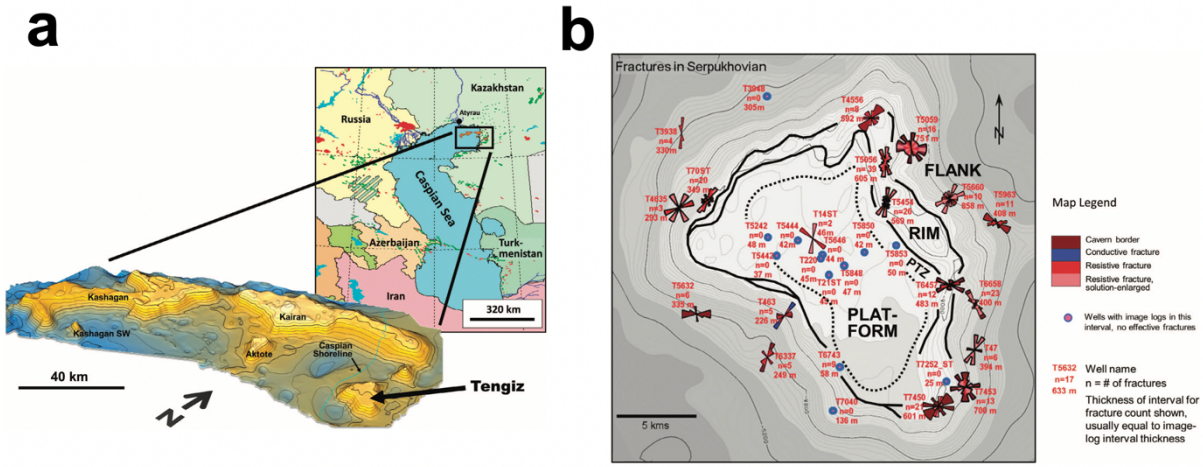

Figure 1. (a) An oblique structural view of Primorsk Archipelago with oil and gas carbonate buildups, with a main focus on Tengiz; (b) Orientation of fractures and caverns in the Serpukhovian strata relative to the PTZ, rim, and flank zones. Both adapted from Collins et al. (2013).

Bolshoi Karatau serves as good analogue for Tengiz Field due to several reasons. However, before addressing the causes, it is important to first clarify the nomenclature of the geological site. The name Great Qaratau is the proper translation of the Kazakh term *Үлкен Қаратау*,

aligning with contemporary Kazakh orthography, and it should ideally be used in modern academic writing. However, for consistency with prior studies conducted during the Soviet Union, this work will adhere to the name Bolshoi Karatau. Bolshoi Kratau, features an isolated platform that developed during the Tournaisian-Bashkirian and a broad Devonian platform with a subsequent backstep. In terms of facies, we observe slope boundstones, muddy to grainy gravity flow deposits, as well as oolitic and skeletal platform facies. Most importantly, both Bolshoi Karatau and Tengiz originated in Kazakhstan (**Figure 2**) and formed around the same time. However, Bolshoi Karatau underwent significant tectonic events (Hercynian deformation): a major fold and thrust belt that developed in the Upper Carboniferous, followed by transpressional events during the Permian and Triassic periods.

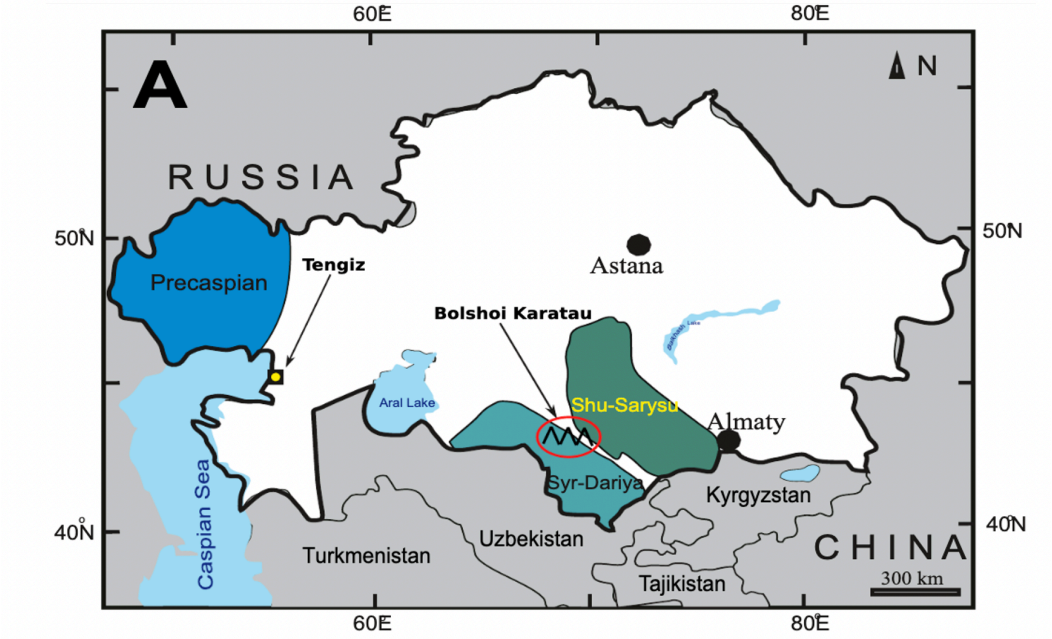

Figure 2. Location of Tengiz and Bolshoi Karatau within the territory of Kazakhstan. Adapted from Umralin et al. (2024)

The fracture data from Bolshoi Karatau might be used for improved reservoir modeling and forecasts. It may help improve the prediction of fracture size, intensity, and the distribution of of fracture properties with respect to facies distributions. Consequently, based on that it can enhance the forecast of passive and active depletion in the outboard middle-lower slope of Tengiz, as well as predict expected fluid movement, such as secondary gas cap formation and long-term water behaviour. Additionally, it may help in optimizing development projects, including high-pressure large step-rate decline, extended reach drilling and enhanced oil recovery. Furthermore, it can help predict optimal well trajectories based on fracture orientation and spacing and determine the potential extent of matrix.

It was stated in Narr and Flodin (2012), fractures at shallow burial that existed prior to significant overburden are major contributors to productivity in the reservoir at Tengiz Field. As an example, Neptunian dykes that formed early in carbonate sequences. Those fractures typically have steep dips and orientations parallel or orthogonal to the local depositional margin. They are most prominent within brittle, boundstone rich facies in the outer platform to upper slope environments. Diagenetic dissolution after burial by migrating fluids has significantly enlarged most of the fractures to form apertures from narrow openings to cavernous voids. Although, such cavernous fractures are crucial in drilling issues with lost circulation, they might yield excellent production potential when successfully identified (Narr and Flodin, 2012). However, since the focus of the study is the lower slope, analogous of which is Baktysai Formation in the Bolshoi Karatau, where the rocks are relatively deep. Hence, this type of fracture is less likely to be observed in the lower slope, instead, burial fractures are of primary interest.

In Ibrayev et al. (2016), burial fractures (also referred to as B-generation fractures) defined as fractures that developed during the lengthy burial of host strata, while in Collins et al. (2013), it is stated that they formed after deep burial. If fractures develop due to overburden and when pore pressure exceeds the minimum principal stress, *sensu stricto* burial fractures are formed. Additionally, there are fractures that may develop during burial but not as a direct result of burial, and these two should be clearly distinguished. In previous studies, well data verified that burial fractures are widespread throughout the reservoir, with more abundancy near the platform rim (Ibrayev et al., 2016). This might be explained as mechanical strength and deformation history difference between the platform rim and interior. Porous platform facies allowed fluid redistribution with compaction, whereas denser and less permeable rim lithologies restricted fluid movement. Most likely, in the more confined zones, localized overpressure conditions decreased the effective stress enough which in turn leads to tensile failure. These burial fractures tend to be mineralized and were filled by precipitates carried in by expelled fluids during burial (Ibrayev et al., 2016). It was noted that burial fractures in Tengiz are filled with calcite or bitumen, and often terminate at stylolites (Collins et al., 2013). However, due to significant tectonic events, identification of the burial fractures (now observed as veins) is challenging. The burial fractures might be reused, and consequently, nowadays we are observing the burial veins.

1.2. Objectives of the Thesis

This study aims to investigate the following objective which are essential for fracture analysis of the Bolshoi Karatau as a well-exposed analog to the Tengiz:

1) It is important first to understand what is meant by burial fractures, since two regions may have the same rock types (limestones and dolomites) and similar structures, yet completely different type of fractures, making the term “burial” to some extent ambiguous.
2) Afterwards, veins present in the Bolshoi Karatau should be divided into sets to organize data and simplify the characterization and analysis stages. These sets should be defined based on a wide spectrum of criteria instead of depending only on a single criterion, such as orientation. According to (Sanderson et al., 2024), although the orientation of veins is one of the most frequently employed criteria, it might vary depending on changes in local stress conditions (Passchier et al., 2021). Additionally, pre-existing structural anisotropy and heterogenity within the rock can influence the orientation (Butler et al., 2006), and fractures may also become reactivated, resulting in similar orientations of veins but with different ages and types (Holdsworth et al., 1997).
3) This is followed characterisation of the veins on their orientation, width, height and intensity. Based on observations we might see that the width of the veins present in all sections are greater that theoretical width which should have been appeared in case of the burial.
4) Finally, the effect of the bed thickness on the fractures should be investigated. It is commonly accepted that there should be a linear relationship between the spacing and bed thickness (Bogdanov, 1947; Huang and Angelier, 1989; Ladeira and Price, 1981), however, in reality different patterns might be observed.

1.3. Scope of the Work

First, a literature review will be conducted, focusing on the geological setting of the region, followed by an overview of geomechanics to better understand the nature of fractures, as well as a review of previous studies on fracture characterization in carbonate rocks. This will be followed by a detailed methodology designed to address the objectives of the study. Subsequently, the concept of burial related fractures will be defined, and basic calculations will be performed based on assumptions and data collected from the outcrops. Notably, fracture data were systematically recorded according to fracture sets. The relationship between fractures and geological controls, like bed thickness, depositional facies, and tectonic history, was examined together with their influence on fracture intensity and aperture observations.

2. LITERATURE REVIEW

2.1. Geological Setting

Bolshoi Karatau mountains are part of the Karatau mountain range (**Figure 3**), which extends across southern Kazakhstan for around 400 km from southeast (SE) to northwest (NW). The Main Karatau Fault, a series of faults trending NW-SE, splits the Karatau mountain range into the mountain ranges of Bolshoi Karatau and Malyi Karatau (Alexeiev et al., 2009; Allen et al., 2001). It was stated by Lisovsky et al. (1992) that the fault is a continuation of the Talas-Ferghana Fault, and which existed prior to orogeny events and also before the mass Devonian carbonate sedimentation events that occurred across the Precaspian through Chu-Sarysu Basins and eventually gave rise to the Bolshoi Karatau carbonate platform. However, Burtman (1964) considers that the first motion along the fault was during the late Paleozoic. Alexeiev et al. (2009) stated that Bolshoi Karatau have experienced three major deformational events (D1, D2, and D3), starting at the Late Carboniferous through Early Mesozoic.

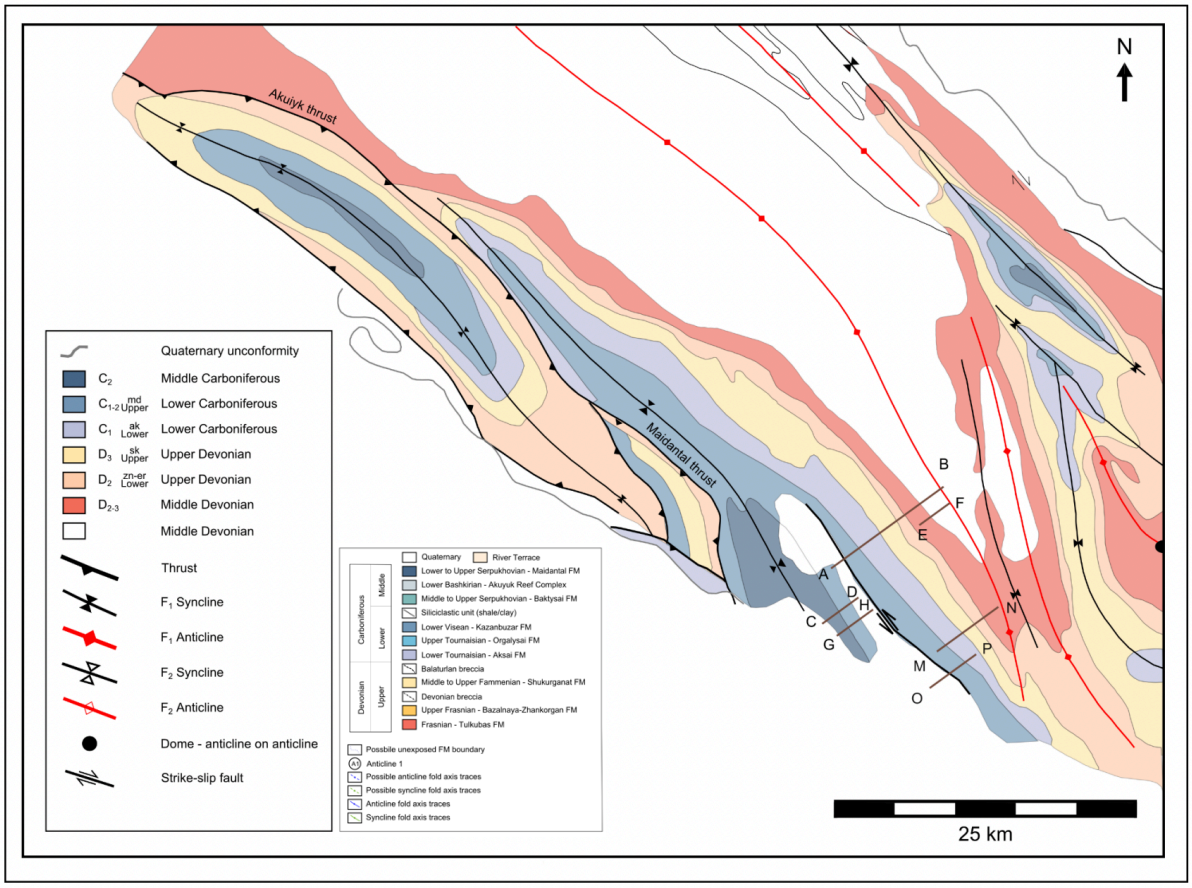

Figure 3. Overview map of the Bolshoi Karatau Mountains. Adapted from Igizgali (2024).

The D1 phase occurred throughout the Bolshoi Karatau, primarily as folding and thrust faulting with an overall NW–SE trend. The recorded folds have a broad range of characteristics, spreading from tight to open folds, and amplitudes varying from 10 m to up to 20 km. Based on Alexeiev et al. (2009), they can be up to approximately 50–80 km laterally. In addition, folds that are related to the D1 phase of deformation tend to have a NE inclination and are commonly overturned, with SW dipping axial planes at steep inclination between 60° and 80°. Minor thrusts and reverse faults are commonly developed on the limbs of folds, with predominantly NE moving displacement. The exception is in the South Akuyuk, where displacement is reversed. Structurally, the Akuyuk Syncline is characterized by two main thrusts: the Northeast Akuyuk Thrust to the NE and the Southwest Akuyuk Thrust to the SW. This is an expression of a passive roof thrust system.

The D2 phase of deformation occurred in the Latest Permian to Triassic periods and tend to be caused by sinistral (left-lateral) strike-slip tectonics (Alexeiev et al., 2009). The regime created a fault network trending NW along with NS trending folds, reflecting the dominant EW direction of shortening. According to on Alexeiev et al. (2009), these D2 faults are either newly formed strike-slip structures or reactivations of pre-existing D1 thrusts, particularly along the North Akuyuk Thrust, where dips are irregular in angle. In case of folding, during D2 it is generally open, with 90° to 120° interlimb angles, and is low amplitude in geometry and truncated by NW strike-slip faults in some regions.

The D3 phase of deformation is attributed primarily to the Triassic and on the basis of the absence of plunging folds in the Jurassic strata. The stage involves dextral (right-lateral) strike-slip faulting with dominant NW trends and EW trending plunging folds, together with a group of subsidiary structures appropriate to NS directed shortening. One of the distinctive structural elements of the D3 phase is the Main Karatau Fault that was disccused earlier. Numerous subsidiary right lateral strike-slip faults also exist, typically with offsets of 2–3 km and in duplex geometries. As stated by Alexeiev et al. (2009), the structural outcomes of the D2 and D3 deformational phases are not uniformly preserved across the Bolshoi Karatau. Both D2 and D3 events predominantly expressed through the refolding of earlier D1 phase structures, which might suggest the development of interference patterns in structurally complex zones which are not observed in Tengiz.

Cook et al. (2002) highlighted three stratigraphic features that makes the Bolshoi Karatau carbonate platform as a great outcrop analog for the Tengiz oil field. To begin with, the

carbonate platforms of both the Bolshoi Karatau and the Tengiz oil field were both formed between 50 and 55 million years ago, beginning in the Upper Devonian and ending in the Bashkirian. Second, it was noted that two regions share similar stratigraphic thicknesses and facies. The Upper Devonian to Lower Bashkirian formations on the Bolshoi Karatau carbonate platform is about 4 km thick, which is comparable to the Tengiz oil field, where seismic profiles demonstrate approximately 3.5 km interval. Furthermore, the 1.8 km of Tournaisian to Bashkirian shoal-water carbonates on the Bolshoi Karatau closely resemble the 1.6 km of comparable shoal-water carbonates in the Tengiz reservoir. Third, the Visean through Bashkirian strata are well exposed in the Bolshoi Karatau, offering a valuable chance for in-depth geological research. It allows to observe and examine the sedimentological and structural features of the reservoirs, including fracture networks, diagenetic features, and facies variations.

As it was stated earlier, Baktysai Formation represents the lower slope of the Tengiz. The depositional processes on the slope might be realtively similar as the processes withina deep water depositional system which formed in a slope to deep ramp paleoenvironment. Baktysai Formation is exposed across several outcrops, where measured stratigrahic sections range in length from about 100 to 1700 meters and highlighted in the map in **Figure 3**. Accroding to Cook et al. (2002), it consists primarily of black, laminated lime mudstones and wackestones, characteristic of low energy, fine-grained sedimentation. Intensity of fractures varies extensively from one outcrop to another. Some exposures are extremely fractured, whereas others remain considerably unfractured.

2.2. Fracture Studies

Ibrayev et al. (2016) provide an integrated methodology for natural fracture analysis in a giant Devonian-Carboniferous isolated carbonate buildup of the southern Precaspian Basin. Their work focused on the importance of fracture classification, understanding relative differences to diagenetic evolution, tectonic setting, and also reservoir architecture in order to more effectively model fracture-controlled flow systems in complex carbonate system.

They suggest a genetic fracture classification system, dividing the fractures into three major types based on essential field observations, diagenetic alterations, and filling material. The A-Generation (Type A) fractures are described as syndepositional structures, formed at the early stages of diagenesis because of gravity controlled instability and slope collapse mechanisms.

They preferentially form parallel to the outer platform to slope break, consist of steep, irregular, dissolution-enlarged openings, and are generally filled with volcanic debris and early marine cements, and in average with width of 80 mm (**Figure 4**). Their existence is closely tied to zones of extreme lost circulation during drilling, suggesting they have a significant effect on reservoir connectivity and early paths of fluid migration.

The proposed conceptual models are consistent with previous carbonate system analog studies of the Guadalupe Mountains and Canning Basin (e.g., Hunt et al., 2003; Frost & Kerans, 2010; Narr & Flodin, 2013). These studies also emphasized the control of slope instability and progradational margin dynamics on early fracture development.

Figure 4. Photo of a Type A fracture observed in core sheds at Tengiz. Adapted from Cook et al. (2002).

The B-Generation (Type B) fractures, however, are generated due to burial and compaction mechanisms, including the formation of stylolites and vertical loading. The generation has two subtypes: early irregular joints and stylolite associated fractures (**Figure 5**). These fractures are more evenly spread across platform and rim but differ in openness and intensity to accommodate differences in lithology, porosity, and stress regime. While of smaller width (30 mm) and often filled, type B fractures are volumetrically extensive and may affect secondary fluid pathways, especially where there is late-stage dissolution.

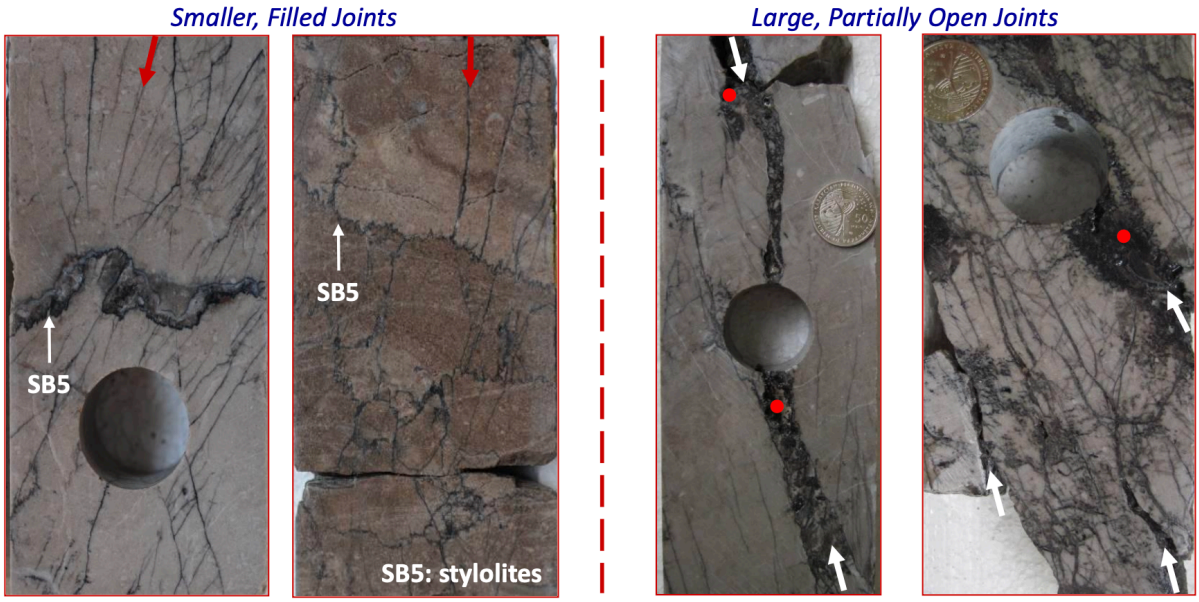

Figure 5. Photo of a Type B fracture observed in core sheds at Tengiz. Adapted from Cook et al. (2002).

The C-Generation (Type C) fractures are the terminal phase of structural overprinting and are associated with late burial overpressure conditions. They are slender, sub-centimeter-scale fractures that are most frequently found in tight lithologies such as boundstones. Though below image log resolution, their density in core and presence in association with bitumen and stylolites show that they both aid in hydrocarbon retention as well as serve as migration barriers.

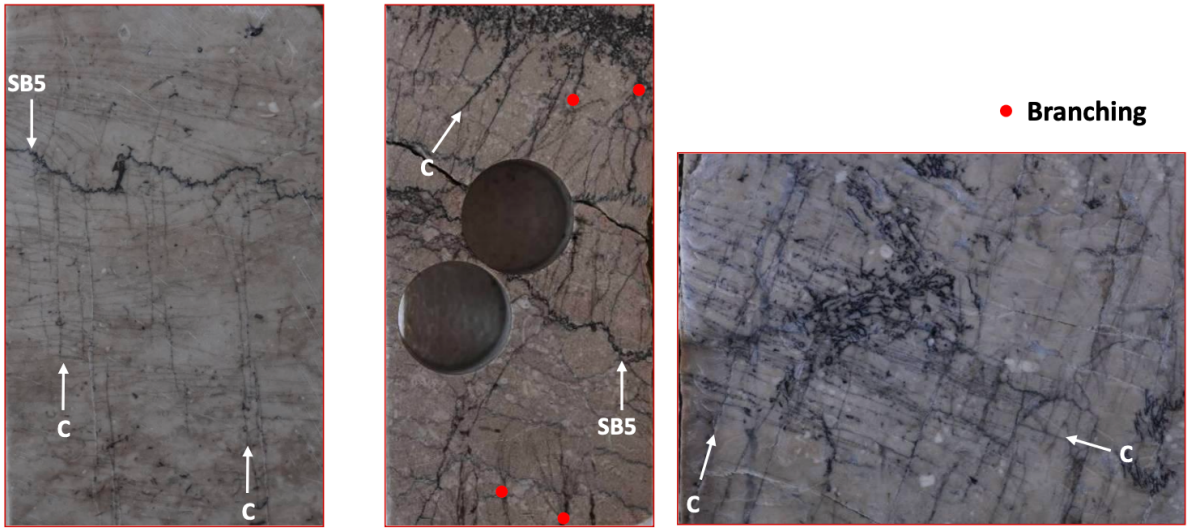

Figure 6. Photo of a Type C fracture observed in core sheds at Tengiz. Adapted from Cook et al. (2002).

Ibrayev et al. incorporated these fractures origins into a structural and stratigraphic model utilizing fine scale core description, borehole image logs, and indirect indicators such as lost circulation zones (LCZs). Importantly, lost circulation data were a significant dynamic dataset

in the absence of good production or well-test data. LCZs in the rim and outer platform zones, particularly in the Serpukhovian sequence are most typically related to type A fractures and karst systems. Platform LCZs are late Visean in age, though, and typically a product of type B fracture swarms. The study suggests excellent spatial control on fracture types and densities, with rim zones being of greater overall intensity and connectivity.

One of the main crucial restrictions which has been responded to by authors is variability in image log quality and availability. Image logs provided good information regarding fracture orientation and resistivity signature and allowed for the differentiation of type A and B fractures in cases, there was no core data available. However, true fracture densities determined from image logs fell short of core derived values by an order of magnitude, which might highlight the requirement for multi source integrated fracture modeling.

Lastly, the Ibrayev et al. (2016) study offers a high resolution and genetically constrained model for the interpretation of natural fracture systems in carbonate reservoirs. Through the integration of fracture origin, diagenetic timing and spatial relationships within stratigraphic and structural domains, it might offer significant predictive potential for characterization of the reservoir. This approach not only assisted in interpreting present day fracture systems but also sets a methodology for fracture classification for analogues studies.

It was said that in layered rocks that vary in different mechanical properties, mechanical bed thickness plays a key role in fracture spacing (Gross et al., 1995; Narr and Suppe, 1994a). Narr et al. (2024) concluded that on the Lennard Shelf, fractures developed relatively early on due to mechanical bedding character and structure of the rock layers around the time they were being deposited or right after deposition.

The veins present in the Bolshoi Karatau Mountains have not been comprehensively investigated, however, similar studies were conducted at other outcrops which also were considered as analogues for the Tengiz.

The recent study led by Narr et al. (2024) focused on Devonian Lennard Shelf carbonates of the Canning Basin. Western Australia. The data was collected across outcrops which represent transitional zones from the platform top to reef flat, reef flat, reef core, upper slope, and middle slope settings. Early fractures that formed syndepositionally, as well as those that developed during relatively shallow burial were considered significant within the scope of the study.

Narr et al. (2024) identified three distinct types of fractures present in the Lennard Shelf outcrops. The first type is early (syndepositional) fractures, which originated after deposition but prior to significant burial. The most common examples are Neptunian dikes filled with seafloor sediments. The second type includes burial fractures, formed after the deep burial of the host strata and filled with marine cement. The third type is late joints, which developed during uplift and exhumation processes.

The relation between the spacing (S), bed thickness (B), and lithology (K) can be expressed as follows (Bogdanov, 1947; Huang and Angelier, 1989; Ladeira and Price, 1981):

$$S = B \cdot K \tag{1}$$

It is commonly accepted that there should be a linear relationship between the spacing and bed thickness. Several explanations have been proposed to define this correlation, and in most cases, it said that there is a direct proportionality between fracture spacing and bed thickness. Hobbs (1967) concluded that mean fracture spacing is inversely proportional to the square of Young's modulus and also a function of the shear modulus of the rock. Ladeira and Price (1981) demonstrated that this linear correlation is reasonably acceptable for tectonic fractures in relatively thin beds. It also was stated by McQuillam (1973) that bed thickness is inversely related to fracture density in a logarithmic way, but not in terms of the structural settings. This might contradict assumptions involving the cause of small-scale fractures with the folding process itself.

Thicker beds are typically contains fewer fractures due to their greater ability to withstand tectonic and sedimentary stress, while thinner beds fracture more easily as they have less structural integrity. Rudstones in high-energy depositional environments, for instance, are produced in thicker, bulkier beds and are less fractured than grainstones, which preferentially form in thinner beds and so are more fractured (Loucks, 1999). Because thicker beds with fewer fractures may act as fluid baffles, and because higher intensity of fractures in thinner beds can increase permeability, this inverse correlation is needed to understand the reservoir quality.

2.3. Rock Mechanics

Understanding and determining the geomechanical properties and in-situ lateral stresses in sedimentary basins are critical in both petroleum and structural geology. This includes a comprehensive analysis of compaction behavior, failure criteria, and fracturing mechanisms,

which are essential for accurately evaluating subsurface conditions and informing effective resource extraction strategies. As sedimentary rocks are subjected to greater burial depths, their properties undergo significant changes. Near the land surface or sea floor, these sediments are typically analyzed using the principles of soil mechanics. In contrast, rock mechanics has traditionally been focused on deeper, more consolidated metamorphic and crystalline rocks.

The key concept to address when discussing rock mechanics is the elasticity, which refers to the ability to withstand and bounce back from deformations produced by forces. The concept of elasticity built upon two key ideas, stress and strain. Stress (σ) is the force exerted per unit area, and strain is a material's response to that force. Mathematically, stress is expressed as:

$$\sigma = \frac{F}{A} \tag{2}$$

where σ is stress (Pa), F is applied force (N) and A is cross-sectional area over which the force is distributed (m^2). There are two fundamental types of mechanical stresses that materials experience under external forces, compressive stress and tensile stress. When a material is pushed together by forces, it experiences compressive stress, which makes it shorter or more compact. On the other hand, tensile stress happens when forces pull the material apart, causing it to stretch or lengthen. Furthermore, based on the orientation of the cross-section towards the direction of the force, if the force is normal to the cross-section, it is called the normal stress. Otherwise, it is it is referred to as shear stress, denoted as τ.

Normally, an underground formation carries the weight of the overlying formations. Hence, the vertical stress at the bottom of a homogeneous column of height z:

$$\sigma_V = \rho g z \tag{3}$$

where ρ is the density of the material and g is the acceleration of gravity. If the density varies with depth, the vertical stress and pore pressure at depth D becomes:

$$\sigma_V = \int_0^D \rho(z) g \, dz \tag{4}$$

$$p_{fn} = \int_0^D \rho_f(z) g \, dz \tag{5}$$

The variations in mechanical properties between rock layers have a significant impact on the development of natural fracture systems. Interpreting fracture networks within these systems

requires an understanding of how stress is distributed across various mechanical layers. A conceptual model was proposed by Bourne (2003), in which he presented elastic stress states within mechanically layered media as a description of fracture development in layered rock. The three-dimensional analytic solutions for an idealized system of bonded, planar, isotropic, homogeneous, linear-elastic layers in equilibrium with a uniform remote stress serve as the basis for the model. Although, there might be some variation of mechanical properties in a same rock type (limestone, sandstone, shale, etc.), the variation within a single rock type is typically much smaller than the variation observed between distinct rock types. Based on that, in order to comprehend the phenomenon that created a complex stress field in the mechanical layers, Bourne (2003) only used two mechanical properties, which stand in for stiff and soft rocks in the mechanical layers.

Certain layers under specific conditions can develop a uniform tensile stress when rock layers are subjected to remote compression. Hence, this might lead to the initiation and propagation of joints throughout these layers regardless of internal thermal contraction or fluid pressure. To illustrate, consider two elastic rock layers that are significantly longer and wider than their thickness and also are able move freely along their shared interface, placed one on top of the other. According to Young's modulus, these two will shorten in the direction of the applied force and reduce in thickness depending on their elastic stiffness under a uniform compressive stress applied perpendicular to the layers. At the same time, based on the compressive strain and Poisson's ratio, the layers will elongate parallel to their planes.

The scenario was modified by Bourne (2003) in such a way that one of the layers is stiffer than the other in both the normal and shear directions. In this case, he suggested that the stiffer layer stretches less along its length compared to the softer layer. However, slip between the layers at their interface balances the difference in stretching by ensuring that the stress within each layer remains uniform and matches the applied stress (**Figure 7A**). Afterwards, Bourne (2003) demonstrated two layers that are bonded together, so no slip occurs at their interface and layer-parallel strain within the two layers is (**Figure 7B**). In this scenario, the stiffer layer experiences extra tensile stress due to the additional elongation imposed by the softer layer, in which the system is balanced and depends on the elastic properties of the layers and their relative thicknesses.

Bourne (2003) stated that initial stress is a type of stress present without elastic strain and arises as rocks develop elastic properties at depth or after complete viscoelastic relaxation.

Consequently, when considering the effect of a uniform initial stress within the layers, both layer-normal and layer-parallel compressive initial stresses should be taken into account. In case of simple layer-normal compressive initial stress, during unloading, the stiff layer thickens less and undergoes less layer-parallel contraction compared to the soft layer. Hence, the soft layer creates a compressive stress within the stiff layer, and the stiff layer demonstrates a tensile stress in the soft layer (**Figure 7C**). These stresses exist even without external loads, and can therefore be defined as residual stresses (Bourne, 2003). According to Holzhausen et al. (1989), residual stresses are another type of stress that exclude body forces and would remain in the system, even if all stresses applied to its boundaries, including thermal stresses, were removed.

In contrast, in case of simple layer-parallel compressive initial stress, during unloading, while the soft layer induces residual compressive stress, the stiff layer generates residual tensile stress (**Figure 7D**). Bourne (2003) also listed other sources of residual stress, including plastic strain (Holzhausen et al., 1989), thermoelastic strain (Savage, 1978) and bonding between grains with different properties (Friedman, 1972).

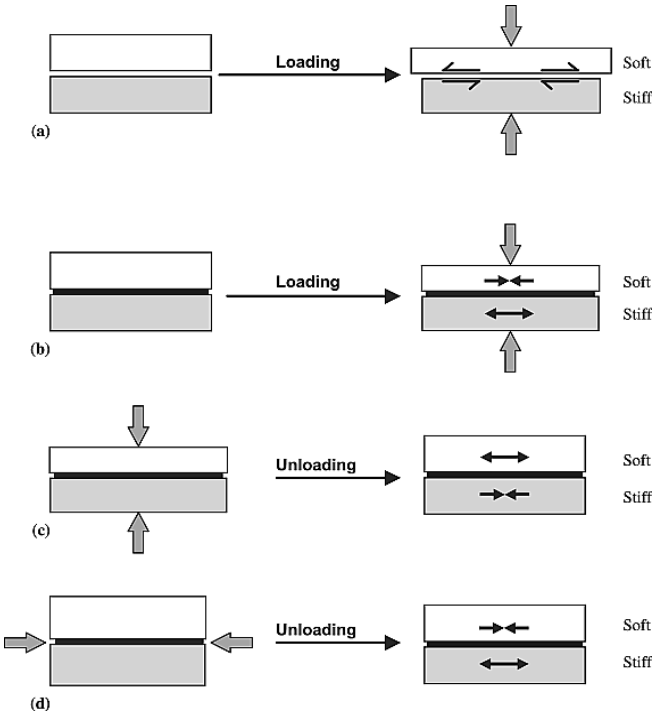

Figure 7. Response of two elastic rock layers, placed one on top of the other, during loading two layers that are nonbonded (a) and bonded (b) together, and during unloading at layer-normal (c) and layer-parallel (d) compressive initial stresses. Adapted from Bourne (2003).

To delve further, Bourne (2003) considered a system of bonded homogeneous, isotropic, linear-elastic planar N layers that are normal to the y axis and have thier own elastic properties and thickness (**Figure 8**). Considering a uniform remote stress acting on the system, a set of governing equations was derived step by step.

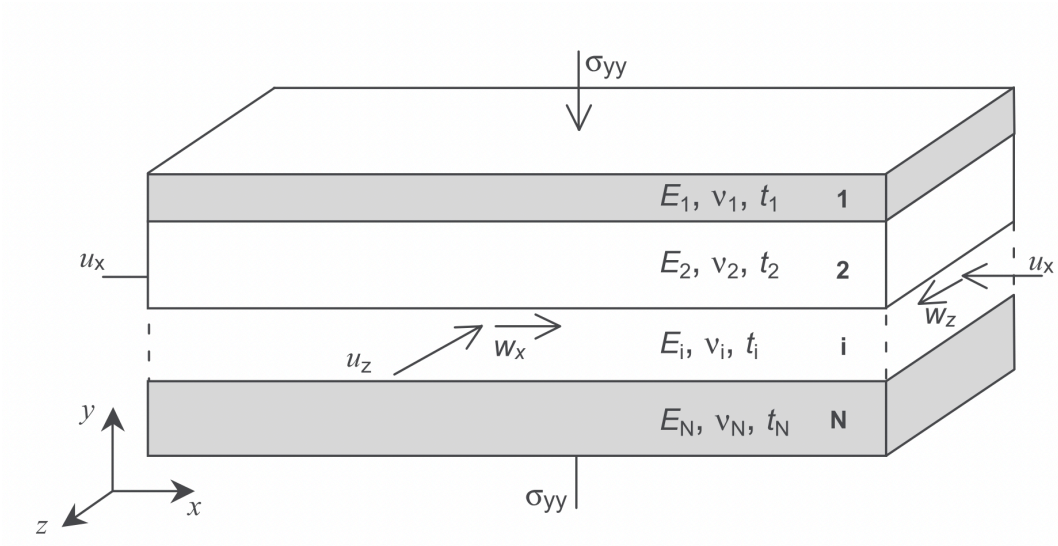

Figure 8. The uniform remote stress acting on the system with N number of layers. Adapted from Bourne (2003).

However, it was stated by Fukunari et al. (2016) that in the Bourne model, the influence of pore-fluid pressure is not considered. In addition, the geological conditions influencing the formation of extension fractures remain somewhat unclear. Hence, Fukunari et al. (2016) proposed modified version of Bourne model to examine the primary factors influencing the formation of extension fractures in the ground and most importantly, to investigate the potential for open mode fractures to form in mechanical layers during basin-burial.

In the revised model for tensile stress generation within mechanical layers under the compressive stress field, Fukunari et al. (2016) demonstrated two cases of strain and stress conditions within the soft and stiff layers subjected to external vertical stress σ_{ZZ}. In the first case (**Figure 9a**), lateral strain is fixed, preventing any lateral elongation of the rock. In contrast, compressive stresses are induced based on the Poisson's ratios of the soft and stiff layers. In the second case (**Figure 9b**), lateral strain is not fixed, allowing lateral elongation of the rock depending on Young's moduli and Poisson's ratios of the layers. Since soft layers have low Young's modulus, they undergo greater elongation and they pull on nearby stiff layers,

where a greater Young's modulus results in less lateral strain. As a result, while compressive stress forms in the soft layer, tensile stress develops in the stiff layer.

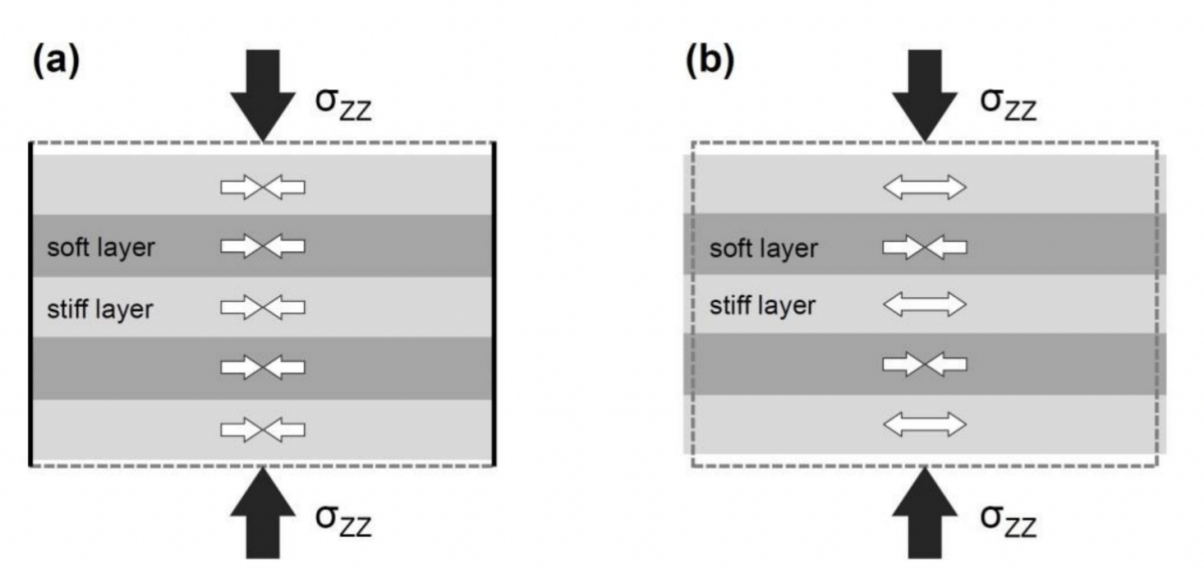

Figure 9. External vertical stress σ_{ZZ} in mechanical layers results in layer-parallel stresses where lateral strain of the layered rock is (a) fixed and (b) free. Note that black arrows indicate external stress, while white arrows indicate internal stress. Adapted from Bourne (2003).

To get analytical solutions for layer-parallel stresses resulting from external vertical, horizontal stresses and pore-fluid pressure, following model geometry depicted in **Figure 10** was used:

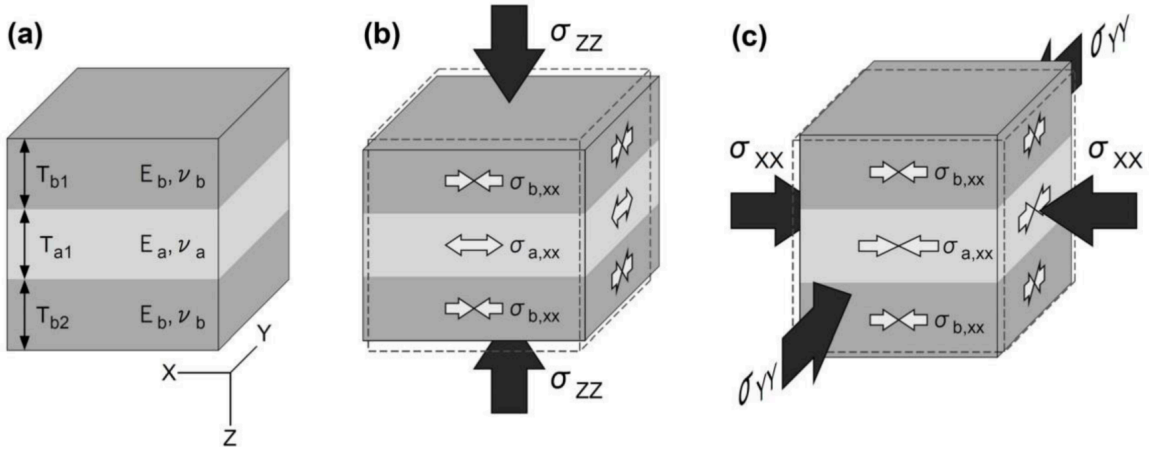

Figure 10. Schematic representations of the three-layer model: (a) Initial state of the layered rock, (b) Internal stresses caused by external vertical stress, σ_{ZZ}, and (c) Internal stresses resulting from external horizontal stresses, σ_{XX} and σ_{YY}. In all three cases there is no slip along the layer boundaries. Adapted from Bourne (2003).

In **Figure 10**, E_a is Young's moduli; ν_b is Poisson's ratios; T_{b1}, T_a and T_{b2} denotes layer thicknesses where b stands for soft and a is for stiff layers; σ_{XX} and σ_{YY} are applied stresses from outside the model in horizontal directions and σ_{ZZ} in vertical direction; and $\sigma_{a,xx}$ and $\sigma_{a,yy}$ are induced horizontal stress in stiff layer while $\sigma_{b,xx}$ and $\sigma_{b,yy}$ are induced horizontal stress in soft layer.

The effective vertical stress (σ_v') in a sediment at depth H under an approximately horizontal seabed can be calculated as follows:

$$\sigma_v' = \rho g H + \rho_w g H_w - P_f \tag{6}$$

where ρ is average total density (including minerals and pore fluid) at depth of H (psia), ρ_w is average density of the water column above the seabed, H is thickness of the sediment column, H_w is water depth and P_f is pore fluid pressure at depth H.

This equation assumes that there is no substantial lateral variation in the compression modulus (areas with harder or softer spots), which would otherwise lead to a redistribution of vertical stresses, creating stress concentrations and stress relief along a horizontal plane. Any variations in the average density (ρ) can lead to changes in σ_v' at a given depth. The horizontal effective stress induced by gravity at a point is statically indeterminate. In geomechanics, his is commonly expressed as a coefficient K, multiplied by the vertical effective stress:

$$\sigma_h' = K\sigma_v' \tag{7}$$

where σ_v' and σ_h' represent the principal effective stresses when the seabed is considered horizontal.

Drawing on the fracture initiation criterion proposed by Griffith (1924), Fukunari and Gudmundsson (2016) demonstrated the relationship between induced horizontal stresses and effective external vertical stress which highlights the two-dimensional effective stress states in both stiff and soft layers required for the formation of extension fractures:

$$(\sigma_{zz} - P_f) - \sigma'_{stiff,xx} < 4TS_{stiff} \tag{8}$$

$$(\sigma_{zz} - P_f) - \sigma'_{soft,xx} < 4TS_{soft} \tag{9}$$

Here, TS represent the tensile strengths of the stiff and soft layers. During the formation of extension fractures, σ'_{xx} will be equals to negative value of the tensile strengths which indicats that the effective vertical stress must be less than 3TSa for the stiff layer and 3TSb for the soft layer at that time. Therefore, the following stress conditions must be satisfied during extension fracture formation:

$$\frac{\sigma'_{\mathrm{stiff,xx}}}{(\sigma_{zz}-P_f)} < -\frac{1}{3} \tag{10}$$

$$\frac{\sigma'_{\mathrm{soft,xx}}}{(\sigma_{zz}-P_f)} < -\frac{1}{3} \tag{11}$$

The subsequent step involves gaining an understanding of failure mechanics, in other words, the processes of fracture initiation. In general, when significantly large stresses are applied to a piece of rock, the likelihood of failure occurrence is significant. The strength of a rock is often defined as the stress level at which it usually fails, and it is measured using uniaxial (unconfined compression) or triaxial (confined compression) tests. Referring to **Figure 11**, we can observe that there are several important concepts are depicted. To begin with, there are three distinct regions: the elastic, ductile, and brittle regions. The rock deforms elastically in the elastic region before returning to its initial state when the stress is released. The sample experiences permanent deformation in the ductile region (might be small in practice), but it is still able to sustain loads. On the other hand, as deformation increases in the brittle region, the specimen's capacity to tolerate stress rapidly declines. In addition, the peak stress denoted as uniaxial compressive strength, while the yield point is the point at which permanent deformation takes place. The stresses felt by the solid framework that result in failure are called as effective stresses (σ').

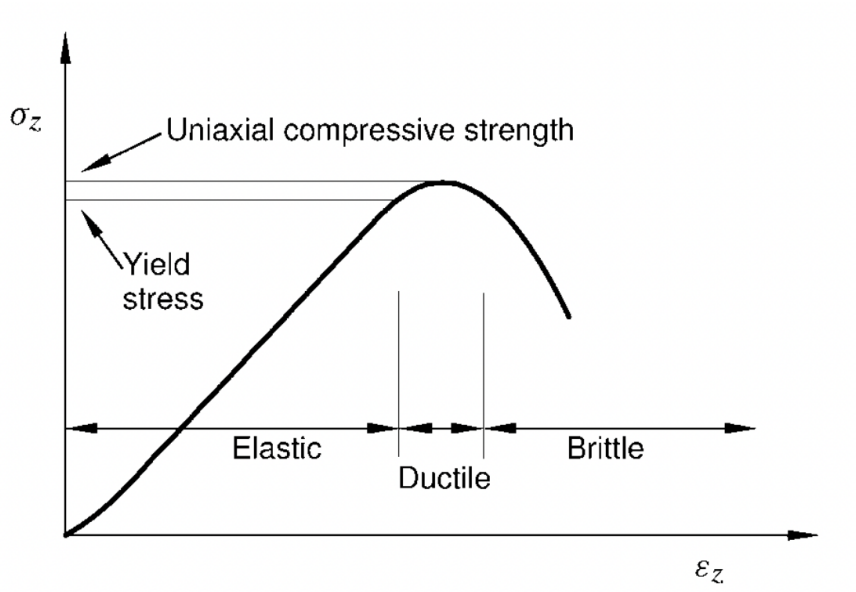

Figure 11. Schematic illustration of stress against deformation in a uniaxial compression test. Adapted from Khamehchi et al. (2024).

The failure surface may be described by the three principal stresses (σ'_1, σ'_2 and σ'_3). Conventionally, the relation represented as $\sigma'_1 \geq \sigma'_2 \geq \sigma'_3$. For the simplicity, the failure surface in two dimensional stress space is considered, where the focus is on the influence of the largest (σ'_1) and smallest (σ'_3) principal stresses.

3. METHODOLOGY

3.1 Sampling Information

Three outcrops were selected which are located within the Baktysay formation: Aktobe and Akuyuk. For the evaluation of the sections, the accessibility of these locations and their degree of coverage were also considered. The Aktobe section is a short outcrop situated on the southwestern limb of the big syncline. There are three geological formations within the section, namely Baktysai, Akuyuk Reef Complex, and Maidantal. Althought, multiple studies have been carried out in the Aktobe section (Belka et al., 2021; Cook et al., 2002; Zhaimina et al., 2014), the fracture system of the locality has not been investigated. Same for the Akuyuk section. Akuyuk section features prominent white cliff-forming units that have been reffered as a reef (some as mud mound) complex. In contrast, the darker-colored strata beneath these units have not been studied well. Classification was performed based primarily on their darker appearance and lower stratigraphic position, and identified as deep-water facies (Cook et al., 2002).

The number of scanlines for each section: Aktobe – 12 and Akuyuk - 5. Each scanline consists of measurements varied between 19 to 138 fractures. In total 998 vein measurements were performed. For each section, drone photo models were captured and later analysed.

3.2 Measuring Procedure

In all three sections, beds with abundant veining were selected for scanlines, while neglecting those with few veins. In addition, beds covered with lichen and weathered surfaces were excluded from the study.

After selection of the beds, a measuring tape was placed along an exposure, parallel with bedding, and all intersecting veins longer than 10 cm in height were captured. The offset of 10 cm was selected to systematically measure the data, as veins with smaller height might be continuations (or wings) of the bigger ones. The numbering fractures started from the 0 and went along the measuring tape. To begin with, the position of the veins was indicated, followed by the measurement of orientation, including the dip azimuth and dipping angle. Afterwards, the width values of the fractures were measured by using an aperture card with a minimum width of 0.05 mm. The upper and lower height and length of the fractures were captured with their terminations. Six possible terminations were identified: bed (B), fracture (F), stylolite (S),

tips out (O), cover (C) and out of outcrop (OUT). **Figure 12** and **Table 1** provide elaboration on the terminations. In the scheme, orientation of the bedding and scanline are 000/00 and 180/90, respectively. Scanline direction is 090-00. Type of the veins were examined based on their behaviour: extensional, shear, normal, reverse and strike-slip. This was followed by identification of the shape: planner, curved and irregular. Finally, based on all collected data and observations, sets were assigned for each vein. In cases, where it was challenging to measure or uncertainties were present, these data were noted in the comments section of the scanline sheet which is presented in the (**Appendix A**).

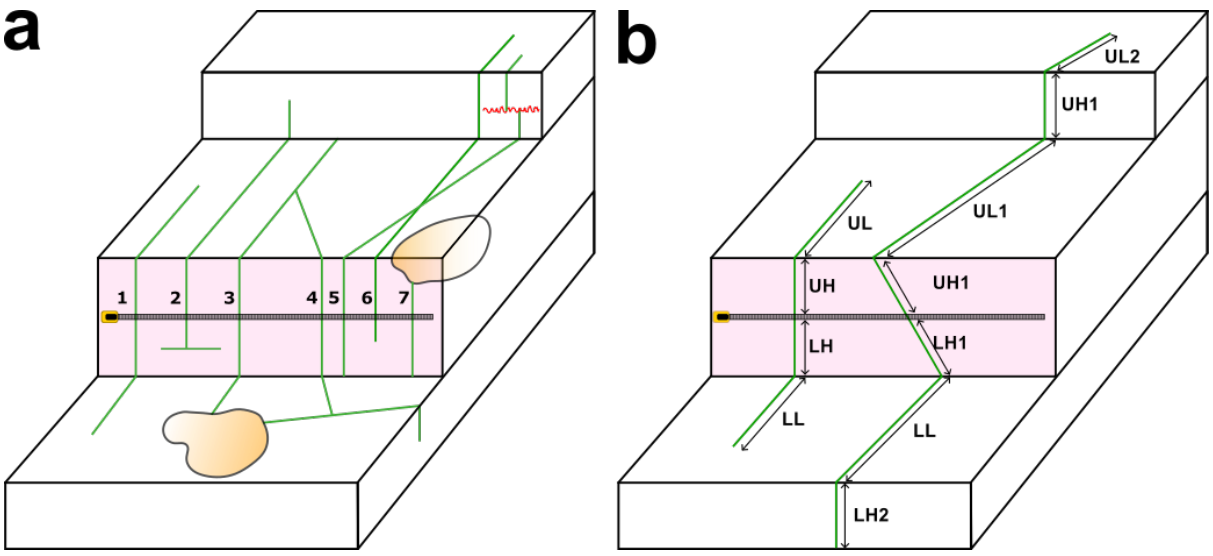

Figure 12. The first scheme of horizontal bedding (a) illustrates different terminations of veins, while the second (b) shows how the height and length of the veins were measured. Green lines represent veins with their upper and lower terminations. The pink line denotes the bedding plane where the scanline was placed. The yellow areas represent covered regions (lichens).

Table 1. Upper and lower height and length variations of seven different veins depicted in **Figure 12**.

Vein #	Upper height termination	Lower height termination	Upper length termination	Lower length termination
1	OUT	OUT	O	O
2	O	F	OUT	-
3	OUT	OUT	B	C
4	OUT	OUT	F	F
5	S	B	OUT	-
6	OUT	O	O	-
7	C	B	-	-

For digital photo models DJI Zenmuse X5 a high-quality camera designed specifically for aerial photography was used for Matrice 200 Series V2 drone (China) and later models were created in Autodesk Meshmixer (Version 3.3, United States).

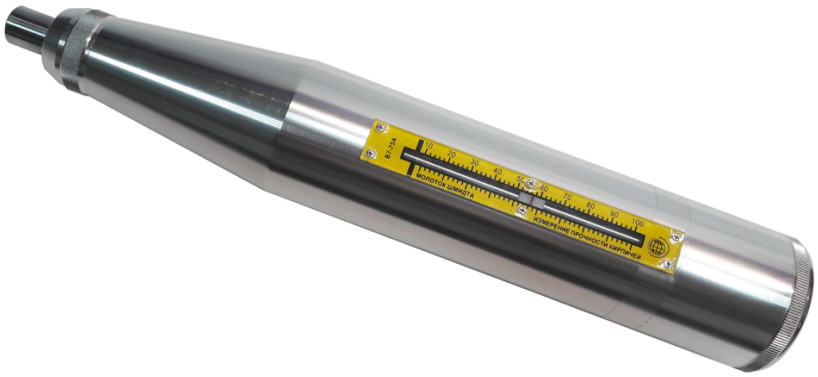

Figure 13. A Schmidt hammer (75A) manufactured by Восток 7 employed for testing.

A Schmidt hammer (75A) from *Восток 7 (***Figure 13***)* was used to determine the compressive strength of carbonate rocks in the outcrop based on rebound values. Rebound measurements were taken systematically on bedding. Surfaces of the rock were cleaned by initially removing loose, weathered debris prior to taking each measurement. The hammer was perpendicular (90°) to the rock face and away as possible from the edges, fracutues and chert layers. However, in some instances, measurements were close to the mentioned areas due to the unavailability of flat and clean surfaces. In addition, at least 3 readings were taken at each position to obtain a representative average rebound value. These data later were utilized to convert to Young's Modulus values (Sachpazis, 1990).

3.3 Analytical procedure

Orientation distribution of the veins was measured and represented in stereo plots; vein spacing, vein width, vein length, vein height was measured in scan lines of 6.0 ± 2.0 m long and statistically analysed.

Collected data is processed using Stereonet 11.0 (Rick Allmendinger's Stuff, United States). Veins with similar orientations were grouped into sets. Poles for each fracture orientation were calculated by applying simple trigonometry. Regional and local fold axes were also plotted and the relationship with great circles (vein orientation) were analysed to propose the origin of vein.

To establish principal stresses, three mutually perpendicular stress components acting on a rock mass, cylindrical best fit was determined, and intersection point was centred by rotating the stereonet. Consequently, stress components were identified. All plots were performed in the lower hemisphere of the stereonet.

The number of veins per meter, or fracture intensity, for uncovered beds was calculated by dividing the number of veins by the distance over which the veins were recorded. Similarly, the cumulative vein width per meter was determined by dividing the sum of the vein widths by the measured distance.

4. RESULTS AND DISCUSSION

4.1. Geological conditions for burial fracture formation

As discussed earlier, the first step is to understand the nature of the burial fractures that are intended to be found in the Bolshoi Karatau. To do so, basic calculations should be performed. The formation of burial fractures *sensu stricto* are assumed to develop because de Poisson ratio (ν) of rocks. As vertical loading increases, lateral contraction may initiate tensile stresses strong enough to create fractures. In the absence of external tectonic stresses, such as those associated with regional compression or extension, the horizontal stress (σ_h) in a subsiding platform where sediments are progressively buried due to continuous sedimentation tent to be less than the vertical stress (σ_v). The relation between the horizontal and vertical stressed is expressed in the following way:

$$\sigma_h = \frac{\nu}{1-\nu}\sigma_v \quad (1)$$

According to Dong et al. (2021), a typical value in Poisson ratio for limestone varies between 0.1 – 0.3. Taking the average value of ν = 0.2 gives:

$$\sigma_h = \frac{0.2}{1-0.2}\sigma_v = 0.25\sigma_v \quad (2)$$

Notably, this calculation does not consider compaction or sliding of grains during the burial, hence σ_h would be increased. Under these assumptions, taking an average density (ρ) of the rocks of 2400 kg/m^3, an acceleration of the gravity field (g) of 10 m/s^2 and H as a depth in km, the vertical stress (MPa):

$$\sigma_v = \rho g H \approx 24H \quad (3)$$

If the rock is porous and water saturated, the pore fluid pressure (p_f) at this depth would be roughly 10 MPa which exceeds the horizontal stress. This condition allows the development of burial fractures which typically form perpendicular to the least principal stress, in this case horizontal stress.

Considering a 1 m wide rock block at 1 km depth with the same stress and pressure conditions:

$$\sigma_{v\,\text{at 1 km}} = 24\ \text{MPa} \qquad \sigma_{h\,\text{at 1 km}} = 6\ \text{MPa} \qquad p_{f\,\text{at 1 km}} = 10\ \text{MPa}$$

Since the pressure of the fluid is greater than the horizontal stress, a fracture will open in the parallel to the vertical stress direction. In case one fracture appears at the centre of this 1 m wide block, water enters and continues to extend the fracture width (Δx). The fracture will continue to open until the effective horizontal stress will be equal to the fluid pressure. The fracture width might be defined as the difference in horizontal strain between the state at 1 m of block length. The horizontal elastic strain (ε_h) is determined in the following way:

$$\varepsilon_h = \frac{1}{E}[\sigma_h - \upsilon(\sigma_h + \sigma_v)] \quad (4)$$

where E is Young's modulus, obtained from the rebound values of the rocks measured in the field using the cylindrical Schmid Hammer (75A). An average rebound value of $R = 51.59 \pm 6.35$ was obtained from measurements taken across Aktobe and Akuyuk sections (**Table *2***). Separately, similar results were obtained for the two sections: $R = 52.16 \pm 6.35$ for Aktobe and $R = 50.85 \pm 6.51$ for Akuyuk. Afterwards, the regression equation (**Equation 5**) presented in Sachpazis (1990) was applied:

$$R = 0.51549\,E + 17.488 \quad (5)$$

The value of 66.16 ± 12.33 GPa lies within the typical range of Young's modulus values for limestone (55.1–82.7 GPa) as shown in Lake (2007) and Tsiambaos&Sabatakakis (2004) However, as seen in Table 2 there are values such 43.67 and 92.17 Gpa which fall outside the typical range. These differences might be attributed to several factors scuh as intrinsic rock properties, methods of estimation and the process of data collection. Using the Schmid Hammer offers practical advantages for rapid assessment in outcrop conditions, however, it is also subject to limitations regarding the sensitivity to surface roughness, weathering, moisture content, and fracture planes (Aydin, 2009; Singh et al., 2012). The lower modulus values might reflect localized zones of microfracturing, weathered surfaces, or reduced cementation, while the higher values could be influenced by anomalously dense or well lithified carbonate zones (layers with chert), or overestimation due to rebound enhancement on harder and less porous surfaces. Therefore, while Schmidt hammer rebound-based correlations are valuable for comparative and preliminary analysis, they can give values ranges different from laboratory based uniaxial compressive testing on prepared specimens.

Theoretical width of the fracture is determined by using **Equation 6**:

$$\Delta x = \frac{(1+\nu)(p_f - \sigma_h)}{E} \quad (6)$$

As a result, based on provided conditions, the width would be about 73 μm. When we assume a lithostatic fluid pressure ($p_f = \sigma_v = 24$ MPa), then we obtain a fracture with width of 326 μm.

Now, doing the same calculation with the same values of E, ν and p_f for a depth of 4 km gives:

$$\sigma_{v\ at\ 4km} = 96\ \text{MPa} \qquad \sigma_{h\ at\ 4km} = 24\ \text{MPa} \qquad p_{f\ at\ 4km} = 40\ \text{MPa}$$

In this scenario, the vein width would be 290 μm for water at hydrostatic pressure and 1.31 mm for water at lithostatic pressure. However, it is unrealistic to expect that no compaction and grain migration occurred with burial to 4 km. Therefore, true widths were likely much more constrained than suggested by the estimates. In other words, the width of the burial fractures in the outcrop should not be higher than those values.

However, the width of the veins observed in the field are much larger and it will be discussed in the following sections and several possible explanations might account for this. If there are elevated fluid pressures due to sealing, a fracture widening will automatically result in a decrease in the fluid pressure, as the total volume is enlarged. Without a corresponding enlargement of the water volume, the fracture width cannot be maintained. It is also possible that fractures form during burial and are later reactivated and filled with calcite in a different tectonic or diagenetic environment.

In over pressured zones (typically below depths of around 2 km) where the rocks are sealed, a necessary condition for the build up of water pressures higher than hydrostatic. With these conditions, the water volume is *quasi constant*, and simply widening a fracture would cause pressure to decrease, which prevents further fracture propagation. Fractures can open only when fluid pressure exceeds the minimum principal stress (σ_h), yet if the water volume is constant, then the process is not effective. In such cases, compaction may be required to establish the conditions for fracture, but compaction also increases σ_h, counteracting the process. This raises the possibility that so called *sensu stricto* burial fractures that are not possible in rocks under conditions of high fluid overpressure.

Table 2. Rebound values obtained from different beds in the field using the cylindrical Schmid Hammer and Calculated Young's modulus (GPa) based on Sachpazis (1990)

Section	Rebound values	Calculated Young's modulus (Gpa)
Aktobe	56	74.71
Aktobe	52	66.95
Aktobe	57	76.65
Aktobe	63	88.29
Aktobe	51	65.01
Aktobe	51	65.01
Aktobe	63	88.29
Aktobe	58	78.59
Aktobe	49	61.13
Aktobe	56	74.71
Aktobe	49	61.13
Aktobe	49	61.13
Aktobe	54	70.83
Aktobe	40	43.67
Aktobe	41	45.61
Aktobe	49	61.13
Aktobe	46	55.31
Aktobe	55	72.77
Akuyuk	46	55.31
Akuyuk	43	49.49
Akuyuk	62	86.35
Akuyuk	51	65.01
Akuyuk	53	68.89
Akuyuk	43	49.49
Akuyuk	49	61.13
Akuyuk	53	68.89
Akuyuk	45	53.37
Akuyuk	55	72.77
Akuyuk	48	59.19
Akuyuk	51	65.01
Akuyuk	48	59.19
Akuyuk	65	92.17
Average	**52**	**66**
Standard deviation	**6**	**12**

4.2. Fracture characterizing

Fracture characterization was carried out separately for the Aktobe and Akuyuk sections, since, although both are described as part of the Baktysai Formation, the rock types and fracture systems were different between the outcrops.

Aktobe Section

Twelve scanlines were recorded in the Aktobe section. Based on outcrop observations, strike-slip faults and subhorizontal joints were identified and plotted alongside bedding orientations on the stereonet plot (**Figure 14**). **Figure 14** also illustrates the location of each scanline on the outcrop. The average bedding pole was about at 230-27 which corresponds to 050/63 while the average poles for the strike-slip faults and subhorizontal joints were 337-05 and 054-65, respectively. To investigate the relationships further, the Aktobe section was divided into several segments.

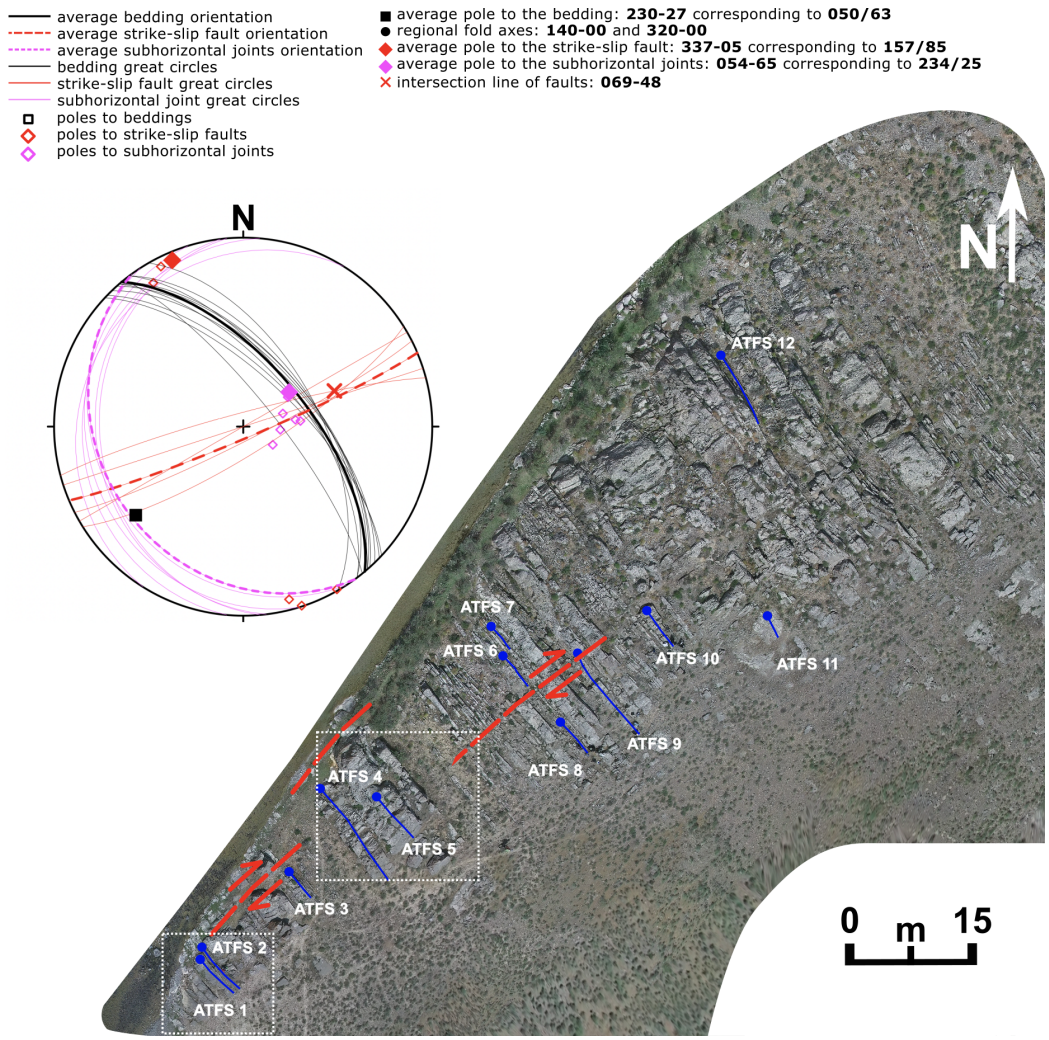

Figure 14. The drone image of the Aktobe section where dextral faults in red and scanline orientation in blue, with circles indicating the beginning of each scanline. The stereonet plot illustrates the orientation of beddings, faults, and horizontal joints within the Aktobe section. The drone image was captured by Zane Jobe.

The first segment (**Figure 15)** consists of two full scanlines and several 1-meter scanlines. Four sets of veins were identified based on their shape, orientation, and width. It is readily apparent that Set AT1 (green) is dominant throughout the outcrop. In addition, two types of en échelon arrays were observed and labelled as AT2 (red) and AT3 (blue) (**Figure 16**). Since they are arranged at an oblique angle to a shear zone, these two were most likely formed due to local faulting events.

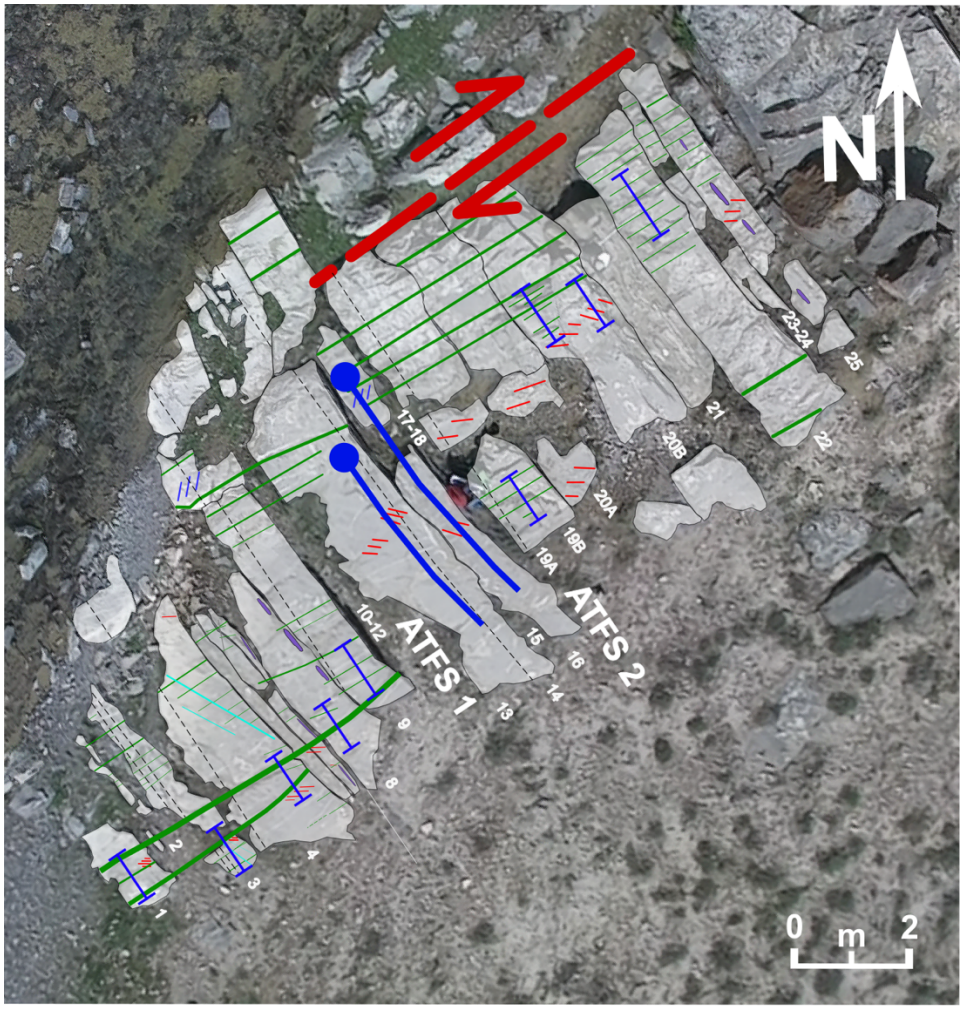

Figure 15. The drone image of the first segment of the Aktobe section with bed numbers, where dextral faults in red and scanline orientation in blue, with circles indicating the beginning of each scanline and lined boundaries demonstrating the 1-meter scanlines. In addition, AT1, AT2 and AT3 set veins depicted in green, red and blue, respectively.

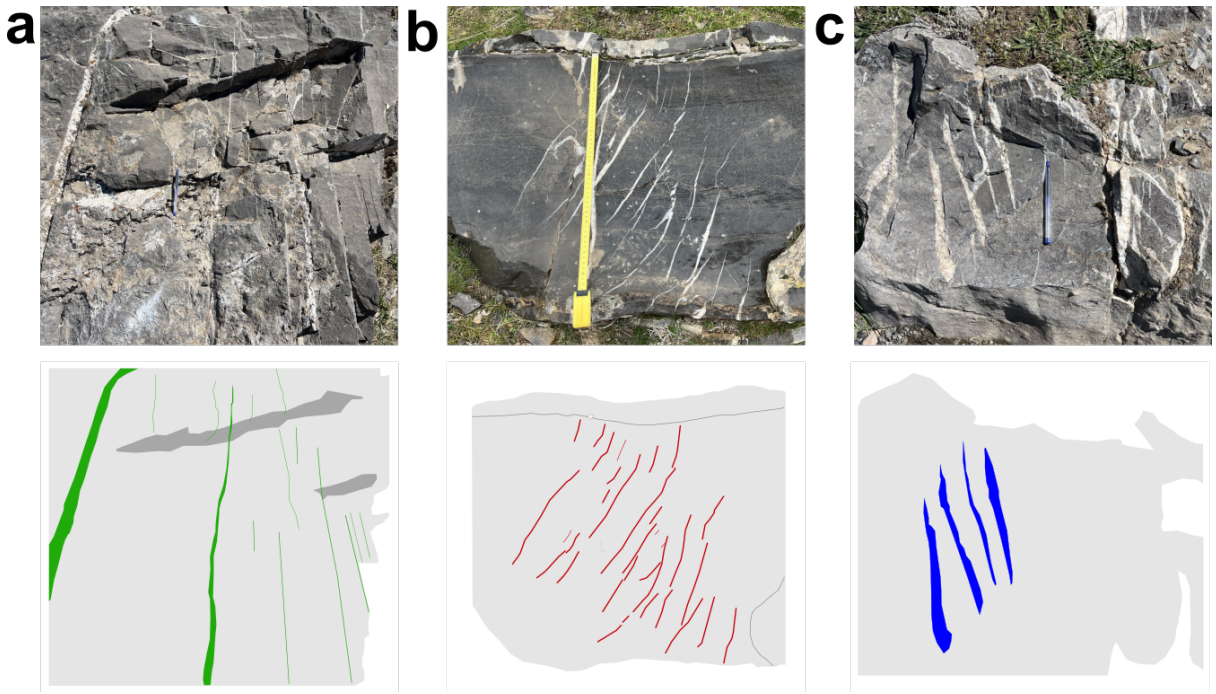

Figure 16. Photo images taken parallel to scanlines in NNW-direction of vein sets with corresponding graphical illustrations from the Aktobe section: (a) AT1, (b) AT2, and (c) AT3.

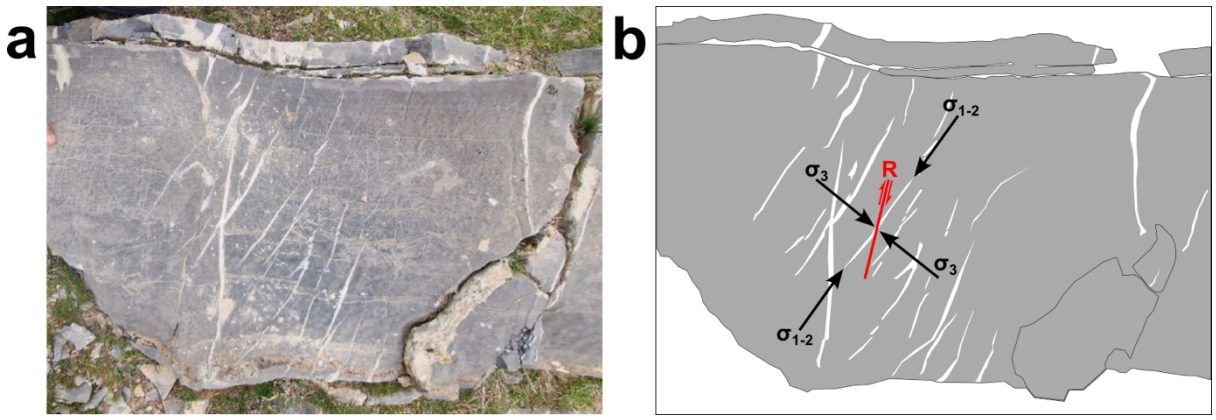

Figure 17. Set AT2 was examined more closely, with an indication of the stress directions.

As it was stated, the strike-slip fault is oriented 157/85, while AT2 veins have an average orientation of 167/75, which places them at an oblique angle of approximately 10 degrees to the fault. In **Figure 17** we might see how tension gashes developed perpendicular to σ_3 (the mininum principal stress) and parallel to σ_1 (the maximum principal stress). They developed perpendicular to the stylolites which develop perpendicular to σ_1 and parallel to σ_3.

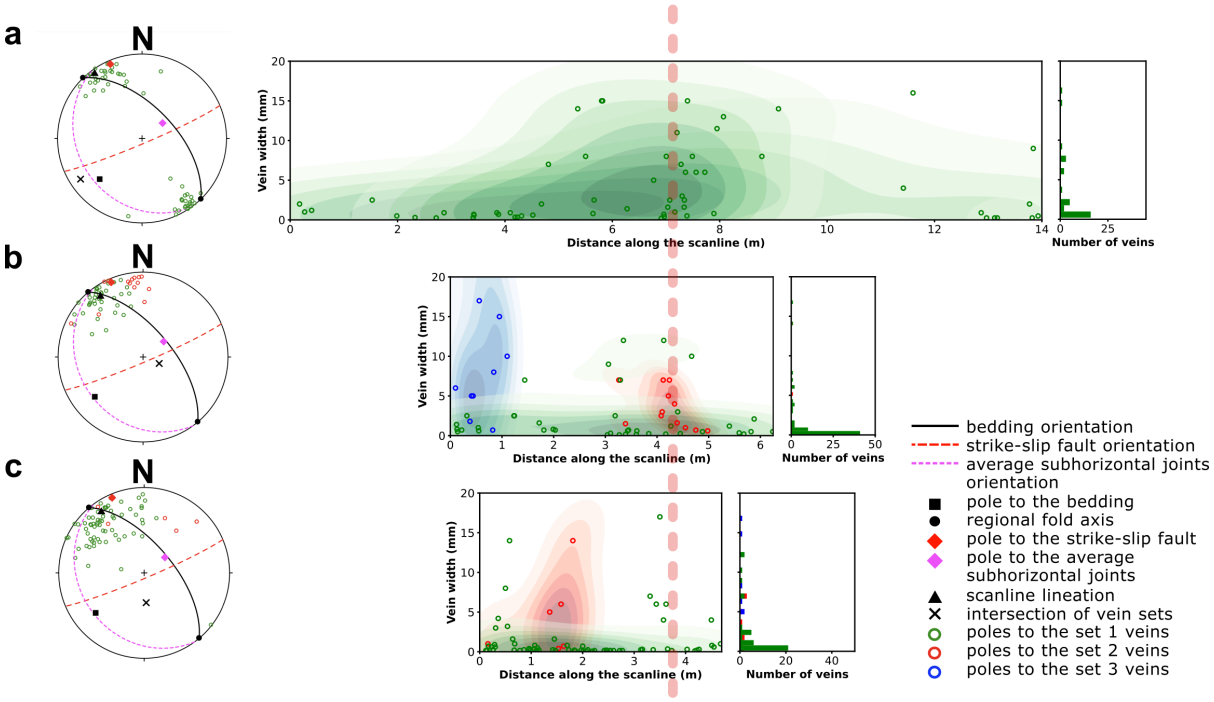

Figure 18. Distribution of vein widths along the scanlines: (a) ATFS 4, (b) ATFS 2 and (c) ATFS 1 with corresponding stereonet plots. The purple dashed line represents the position of the strike-slip fault on scanlines, while the color map illustrates the probability density function based on Gaussian kernel smoothing.

Based on the **Figure 15** and **Figure 18**, we can clearly see the mechanical effect of the fault on veining; there are more veins with greater widths near the faulting zone, in particular the AT2 vein set. Therefore, it can be inferred that the AT2 vein set most likely originated as a result of fault activity (tectonic) which contradicts the interpretation that they are burial veins associated with brittle deformation. A similar conclusion can be drawn for the AT3 vein set, however, this set may have been initiated due to the main sinistral fault. For further investigation, the left side of the fault was also examined (**Figure 19**). However, most beds were either weathered or covered by lichen, leaving only few bed suitable for study. In addition, we still do not know the boundaries of the beds, whether they are defined by stylolite, sedimentological, or tectonic features. Consequently, identifying the terminus of the veins was challenging. The other side of the Aktobe section consists of thick, dominant veins averaging 2 cm in width, oriented perpendicular to the bedding. Some en-echelon array veins were also observed within thick beds of boundstones, consistent with the main Aktobe section.

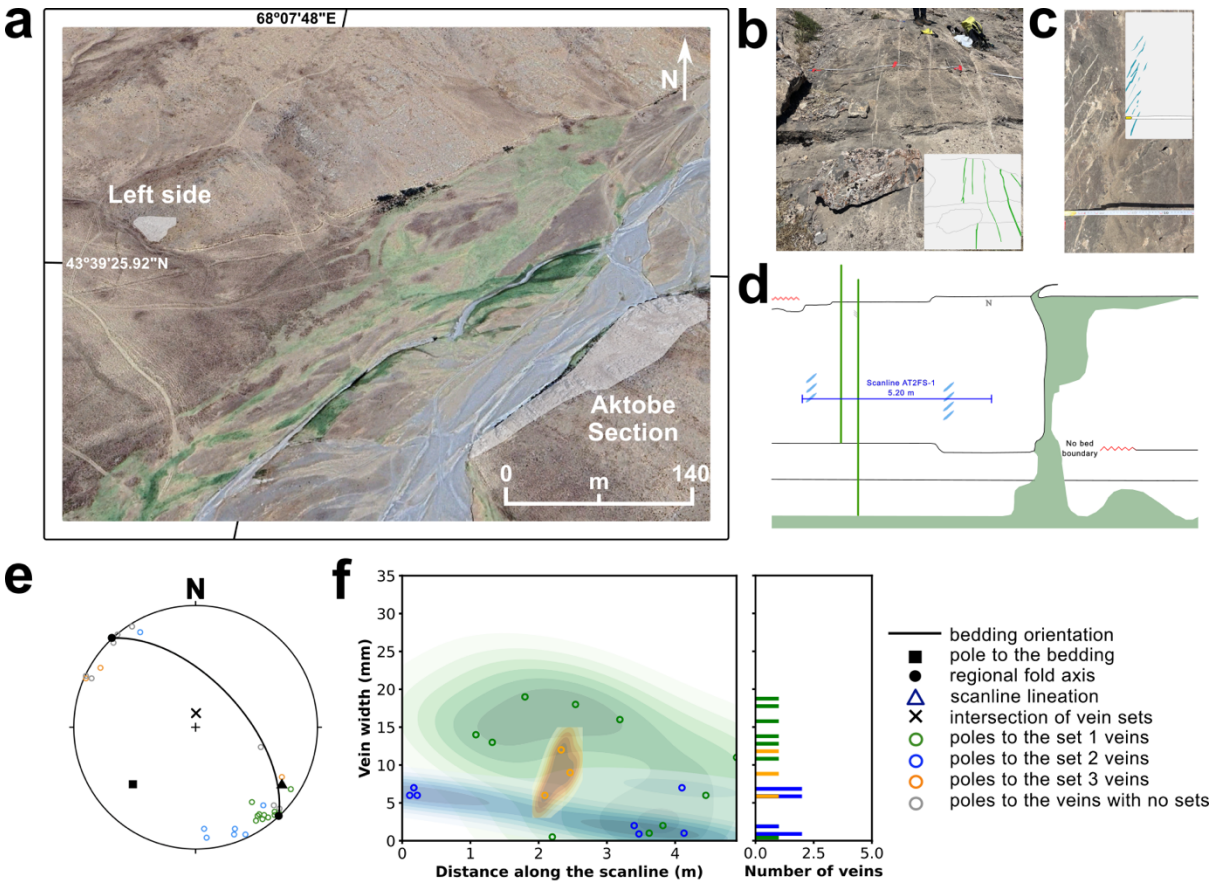

Figure 19. (a) Snapshot of the Aktobe section from Google Earth, indicating the main and left-side outcrops. Photographs of vein sets with corresponding graphical illustrations from the left side of the Aktobe section: (b) the dominant thick LAT1 and (c) en échelon LAT2 vein sets. (d) A schematic view of the bed with the scanline illustrated. (e) The corresponding stereonet plot and (f) the distribution of vein widths along the scanline are also provided.

Akuyuk Section

From 18 measurements taken near the Akuyuk section, the average bedding orientation and pole were derived as 224/50 and 044-40, respectively. The regional fold axes were identified with orientations of 316-00 and 136-00. In addition, an oblique slip (sinistral and normal) fault near the section was determined, with an average orientation of 340/70, while orientation of slickensides was recorded as 068-07 and 257-23 (**Figure 20**). These values were utilized in all subsequent stereonet plots of the Akuyuk section, each associated with its respective bedding orientation.

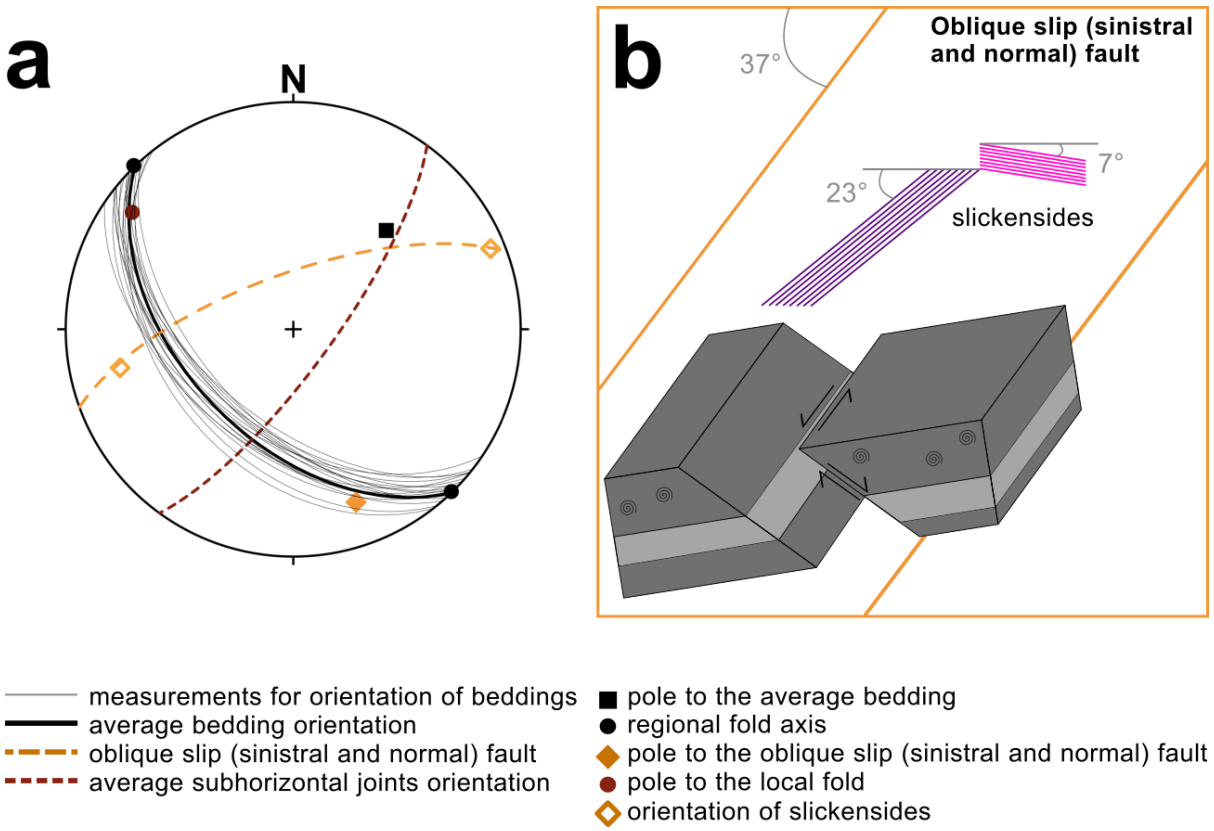

Figure 20. (a) Stereonet plot showing orientation of the beds with dip azimuth and dipping angle values in the Akuyuk section. (b) A schematic representation of fault plane in the Akuyuk section with angles between the slickensides, fault and bedding planes.

In addition to the main Akuyuk section, vein orientations were examined in three nearby regions. Four distinct sets were determined based on their orientation, shape and width. However, the distribution of the sets is non-uniform, as shown in **Figure 21a,b.** Although, all five scanlines (AKFS 1, AKFS 2, AKFS 3, AKFS 4 and AKFS 5) and general outcrop observations indicate that set AK1(green) dominates in the main Akuyuk section, it was not seen in the upper parts of the outcrop. Instead, set AK4 (grey) was detected which has unusual and inconsistent orientation for the main section. Set AK2 (red) also might be seen frequently except the lower part of the section (upper layers of a stratigraphic sequence) where it was replaced by set AK3 (blue). The general data regarding the vein sets is given in **Table 3**. We might note that the bedding pole is nearly same to the intersection pole. The poles of three sets in the main Akuyuk section and the scanline lineation lie on the great circle of the bedding. The only exception is scanline AKFS 5, where data was collected from a bedding plane. Furthermore, the poles of set AK2 align with the great circle of the local folding (**Figure 21c**). Consequently, it might indicate that set AK2 have originated due to the local folding.

Table 3. The average vein orientation, width, and spacing values, along with their standard deviation values for different sets determined in the Akuyuk section.

Vein set	Average orientation	Average vein width [mm]	Average spacing [m]
AK1	342/61 ± 003/6	1.05 ± 0.64	0.127 ± 0.021
AK2	024/46 ± 003/7	0.69 ± 0.24	0.177 ± 0.015
AK3	109/62 ± 014/7	2.87 ± 2.54	0.298 ± 0.256

Based on **Table 3**, we might see that the vein orientation, width, and spacing values for three vein sets in the Akuyuk section show distinct formation conditions. AK1 veins exhibit a NW-SE orientation with a steep dipping angle, while AK2 veins demonstrate nearly N-S with a moderate angle, and AK3 veins are in ESE-WNW direction which also shows a higher deviation in dip azimuth values. In addition, the average vein width varies significantly, where AK3 veins being the widest, which is about 2.87 mm, but also displaying the highest divergence. In contrast, AK2 veins are the narrowest, which is approximately 0.69 mm, with the least fluctuation in the width values. A similar trend might be observed in vein spacing, where AK3 veins are widely spaced (2.982 cm) with big deviation, while AK1 and AK2 veins remain closely spaced, with AK1 demonstrating the most compact arrangement. Therefore, we might say that AK3 veins developed under conditions distinct from the more uniform and systematically spaced AK1 and AK2 vein sets due to the observed differences (**Table 3**). Since poles of the set AK3 close to great circle of the fault, set K3 may be associated with the oblique-slip fault but its relationship remains uncertain.

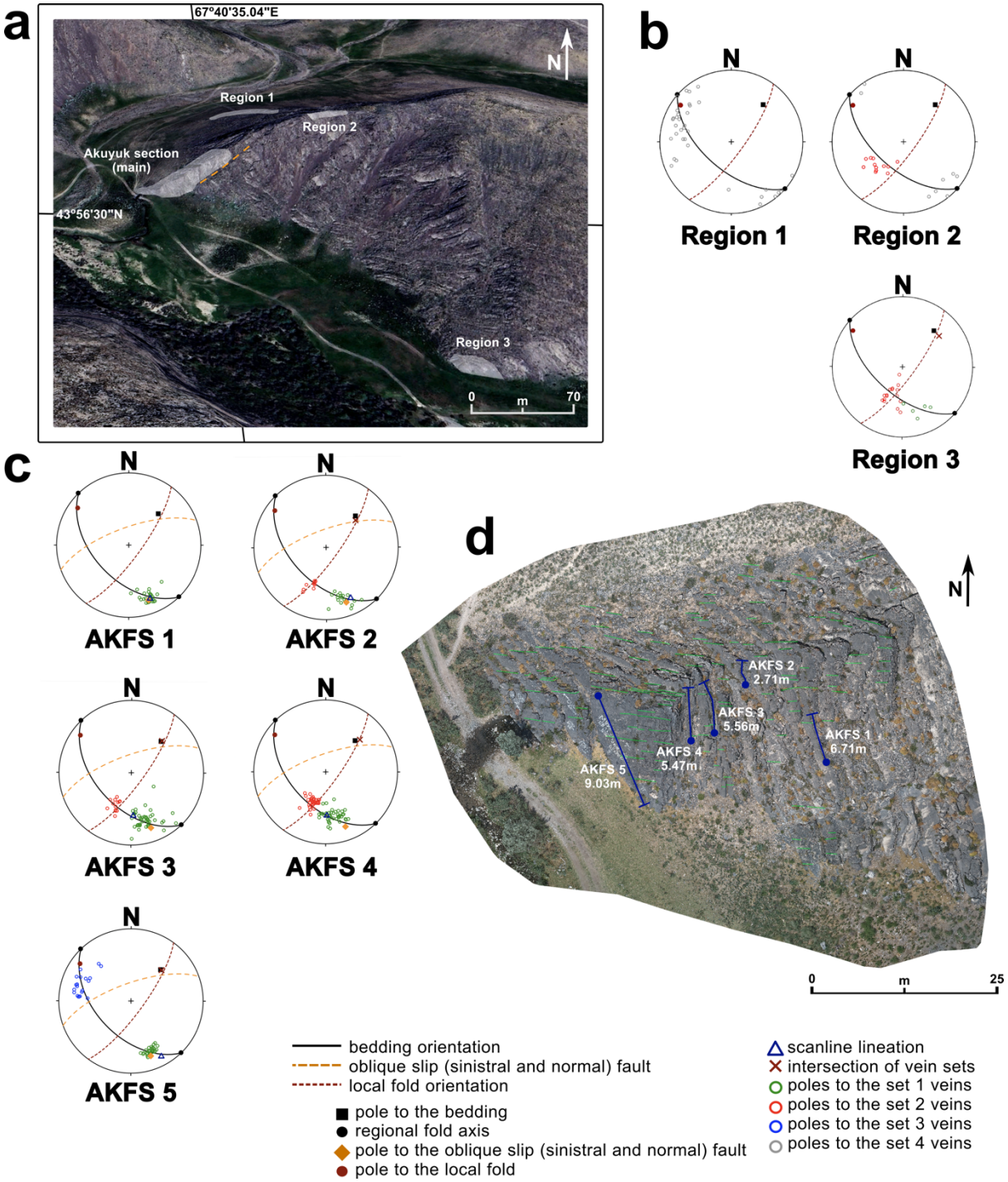

Figure 21. (a) Snapshot of the Akuyuk section from Google Earth. (b) Photo model of the Akuyuk section, with placement of scanlines in blue lines, with circles indicating the beginning of each scanline (drone photo model was made by Zane Jobe).

Based on the cross-cutting relationship between the AK1 and AK2 sets (**Figure 22a**), an right-lateral offset of approximately 0.5-1.0 cm can be observed in the AK1 set, while the AK2 set is continuous. This indicates that the AK1 set fractures are older, consistent with burial-related veins. The same conclusion with left-lateral offset might be asserted for cross-cutting

relationship between the AK1 and AK3 sets (**Figure 22b**). Relation between the AK2 and AK3 sets were not observed.

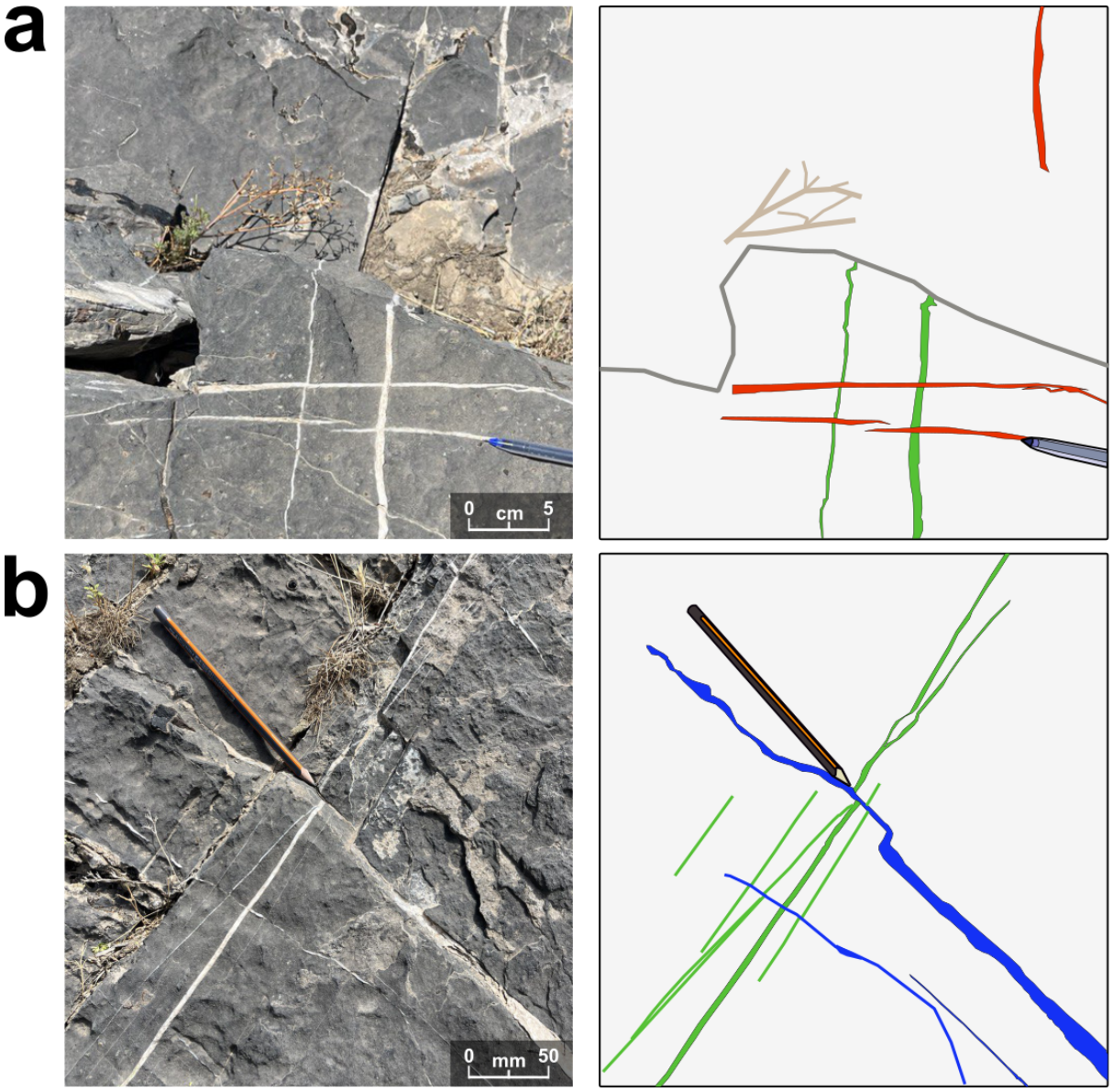

Figure 22. Cross-cutting relationship between the (a) AK1 and AK2 and (b) AK1 and AK3 sets of veins in the Akuyuk Section.

The southern-west part of the Akuyuk syncline was also investigated, and a single scanline was conducted (**Figure 23**). To compare the northern and southern parts, all stereonet plots were rotated along the fold axis so that the bedding on both limbs is parallel (the fold was unfolded). In **Figure 23**, we might observe both limbs contain set AK1 veins which possibly indicate that set AK fractures were originate before the foldling.

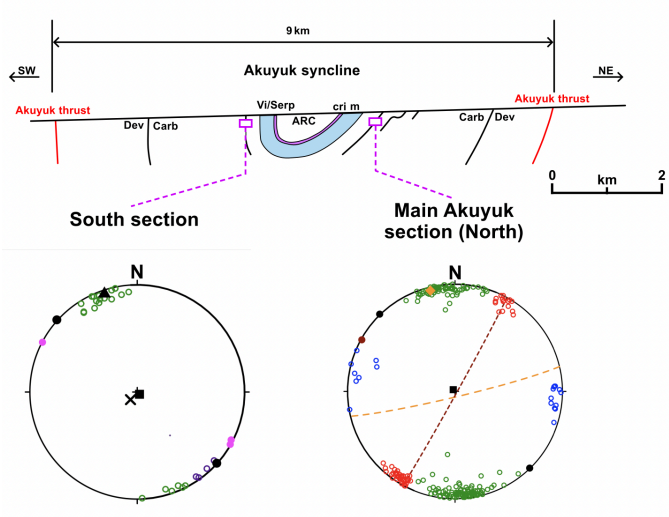

Figure 23. A schematic representation of the Akuyuk Syncline, featuring unfolded stereographic plots of the Southwest and Northeast (Akuyuk) sections.

Summary regarding the dominant sets in both sections

Table 4. Characteristics of dominant vein sets in Aktobe and Akuyuk sections

Section	Average orientation	Average vein width [mm]	Average spacing [m]	Average height [m]	Calcite vein coverage [%]
Aktobe	150/78 ± 015/09	3.7 ± 1.0	0.2 ± 0.1	0.3 ± 0.1	1.9 ± 0.7
Akuyuk	342/61 ± 003/06	1.1 ± 0.6	0.1 ± 0.02	0.3 ± 0.1	0.4 ± 0.1

Table 4 demonstrates a summary of characteristics of the dominant vein set in both sections. In Aktobe section, the dominant vein set showed an average width of 3.7 ± 1.0 mm, an average spacing of 0.2 ± 0.1 m, and an average height of 0.3 ± 0.1 m in beds of 1.0 ± 0.5 m thick. In Akuyuk section, an average vein width was 1.0 ± 0.6 mm, with an average spacing of 0.1 ± 0.02 m and an average height of 0.3 ± 0.1 m in beds of 0.2 ± 0.1 m thick. The calcite vein coverage, expressed as a percentage of the wall rock for the dominant set, was 1.9 ± 0.7 % in the Aktobe section and 0.4 ± 0.1 % in the Akuyuk section.

In addition, the majority of the observed veins were fibrous, and based on their texture, they likely formed through a crack-seal mechanism. This means that the width visible in many of these veins does not represent the original fracture aperture, but rather the cumulative result of multiple sealing events. These veins were never as wide as they now appear. It is highly

possible that, during a later diagenetic or tectonic phase, these veins underwent partial or complete dissolution. The originally sealed, fibrous veins (**Figure 24**) were replaced by open channels. Importantly, the width of these channels does not reflect the original fracture width, but rather the total thickness of mineralized vein material that was subsequently removed. Hence, in the outcrops we are not measuring the initial fracture but rather the cumulative width resulting from crack-seal vein growth followed by dissolution. It is important to understand since the current channel width is controlled by vein growth and dissolution, not by the original mechanical aperture of the fracture.

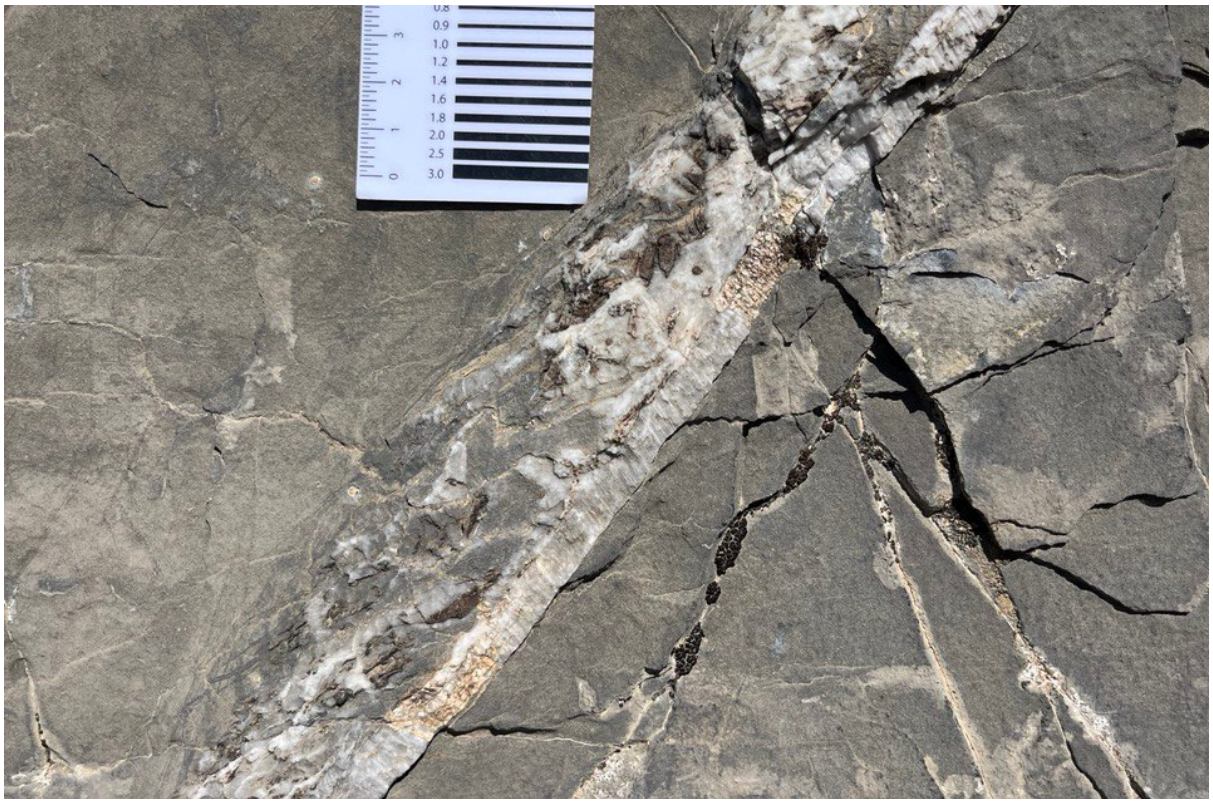

Figure 24. Photo of fibrous vein found in Zhankorgan section.

Based on these observations, the observed veins are not *sensu stricto* burial fractures, nor did they originate during the burial (e.g., due to slope instability), as they are oriented perpendicular to the fold axis and display relatively consistent directional trends. The dominant vein sets in both outcrops were formed during the Hercynian deformation. Moreover, all other vein sets are also attributed to tectonic stresses, as set AK2 and AK3 veins in the Akuyuk section appear to be younger than the dominant set and local fold related, while the tension gashes (set AT2 and AT3) observed in the Aktobe section also originated from tectonic activity.

4.3. Distribution of vein widths

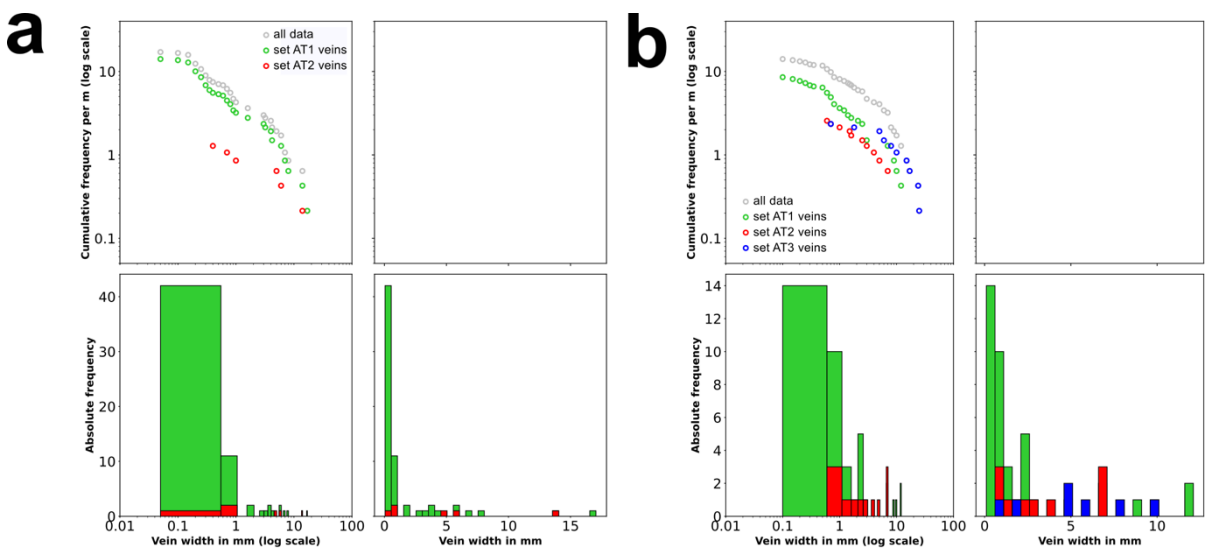

Figure 25. Distribution of widths of vein sets observed in Aktobe section: (a) ATFS 1 and (b) ATFS 2.

Figure 25 illustrates the distribution of vein widths at ATFS 1 and ATFS scanlines using different representations. The top panels are cumulative frequency distributions on a log scale, while the bottom panels are absolute frequency histograms for vein width in both log and linear scales. In both scanlines, the veins are predominantly smaller than a millimeter which is a normal for natural fracture systems developed in low to medium fluid pressure regimes (Laubach et al., 2004). The log-linear character of the relation between the plot cumulative frequencies supports power law distribution. It was stated that this behavior tends to form in multilayered rocks where the fracture growth is governed by mechanical contrasts at bedding or diagenetic contacts (Bai and Pollard, 2000; Narr and Suppe, 1994b).

In ATFS 1 set AT1 veins defines the population as numerous thin veins (mostly smaller than 0.2 mm), an early generation of veins, likely during the first burial or low tectonic stress. Set AT2 veins, fewer in number, but significantly wider and more frequent, imply reactivation or a secondary fracture event under a heterogeneous stress regime (due to the faulting) or high fluid overpressure. In comparison, ATFS 2 shows a denser group of veins, with the addition of set AT3 veins. These are wider in width, with numerous veins greater than 5 mm, suggesting higher strain localization or higher permeability that allowed multiple fluid access. The wider width range in ATFS 2 likewise may be a sign of stronger structural control or stress buildup by mechanical stratigraphy, mostly likely by the fault proximity (Nelson, 2001).

In the Akuyuk section, significant variation in vein width was not observed with the exception of set AK3, which was identified near the top of the succession (AKFS 5). The width of this set was slightly greater than that of the dominant vein set. As previously discussed, there is a likely relationship between set AK3 and fault, which might explain the observed difference in vein width. Furthermore, vein widths in Akuyuk section showed to some extent a consistency along the scanline (**Figure 26**) which was not seen in the Aktobe section. Separate cumulative vein distribution of the section presented in **Appendix B** and **C**.

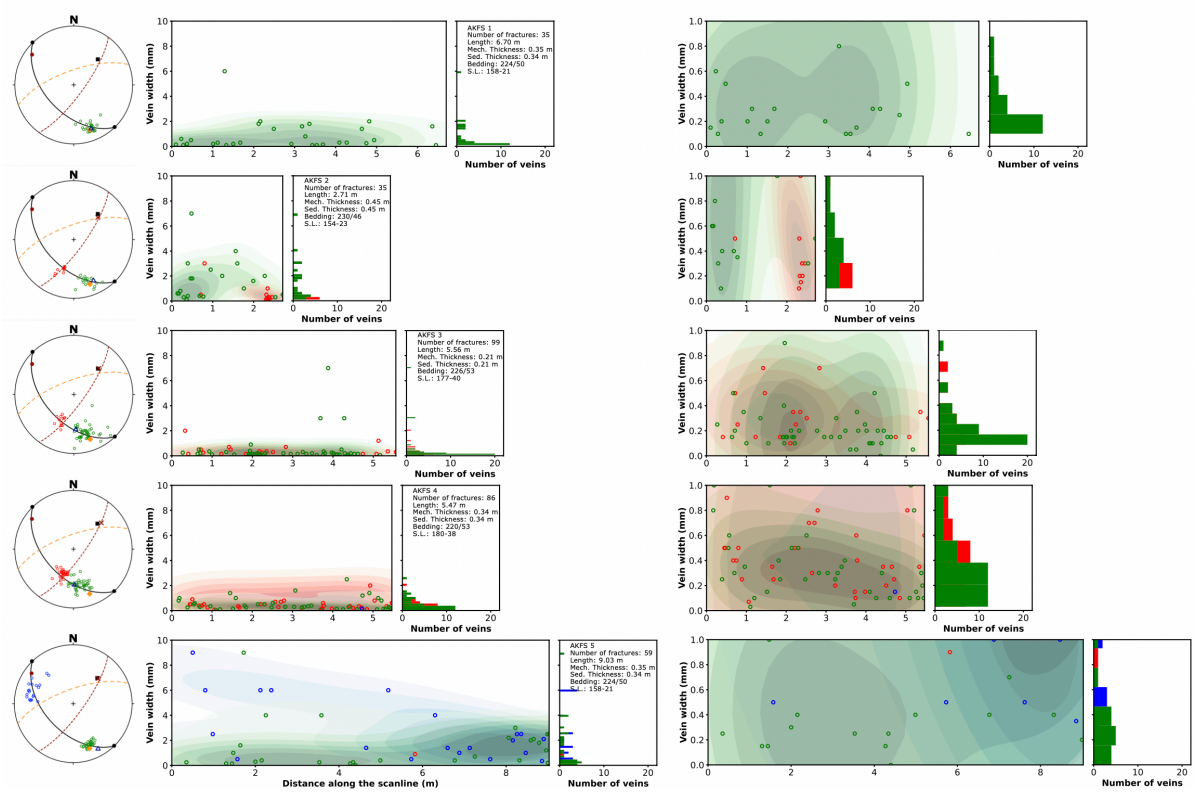

Figure 26. Distribution of vein widths along the scanlines (AKFS 1, AKFS 2, AKFS 3, AKFS 4, and AKFS 5) at different width scales (y-axis), together with the corresponding stereonet plots.

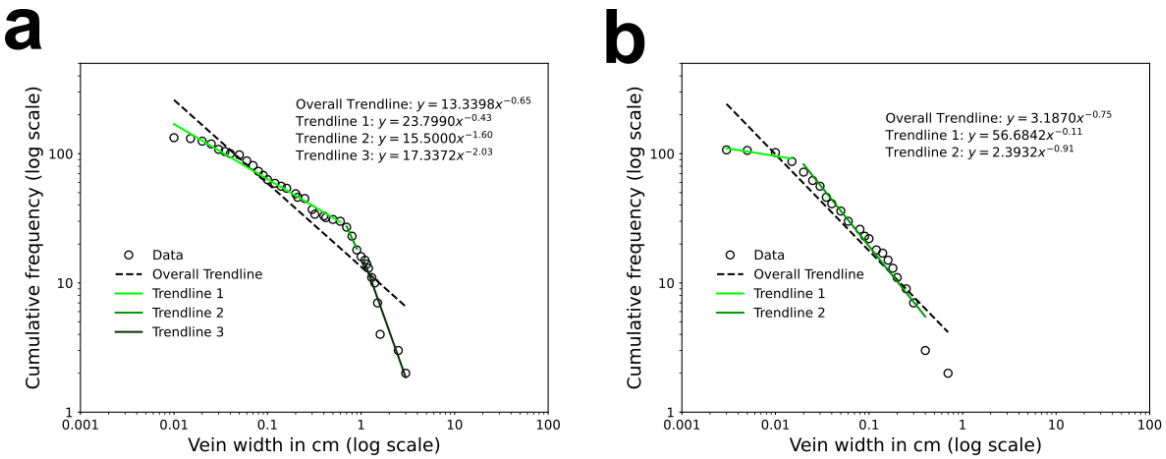

Figure 27. Cumulative frequency of dominant vein widths in (a) Aktobe and (b) Akuyuk sections with indications of trendline equations.

Figure 27a and b show results from the Aktobe and Akuyuk sections, respectively, where dominant vein widths have clear log-log trends. Both sections exhibit multi segmented power-law behavior with segmented trendlines which indicates changes in scaling behavior over width value ranges. The Aktobe section shows more steep slope differences, from gentle slope (–0.43) to high slope (–2.03), showing that the frequency drop-off is steeper in wider veins. The Akuyuk section shows less variable behavior with fewer changes of trend but also scale dependent decline in frequency with slopes ranging between –0.11 and –0.91. For comparison, based on Narr and Flodin studies (2012), the Walnut Canyon Scan W1 data set displays a similar log-log relationship. The slope changes (–0.519 to –3.33) are abrupt, indicating that there is a large fracture width distribution change at large scale. Compared to the Aktobe and Akuyuk sectors, the Walnut Canyon data ranges a larger array of width values, with a clearer separation between small scale and large scale fracture (vein) regimes. These segmented patterns in all three sections suggest that fracture and vein development is controlled by variations in stress fields, fluid pressures, and lithological heterogeneity.

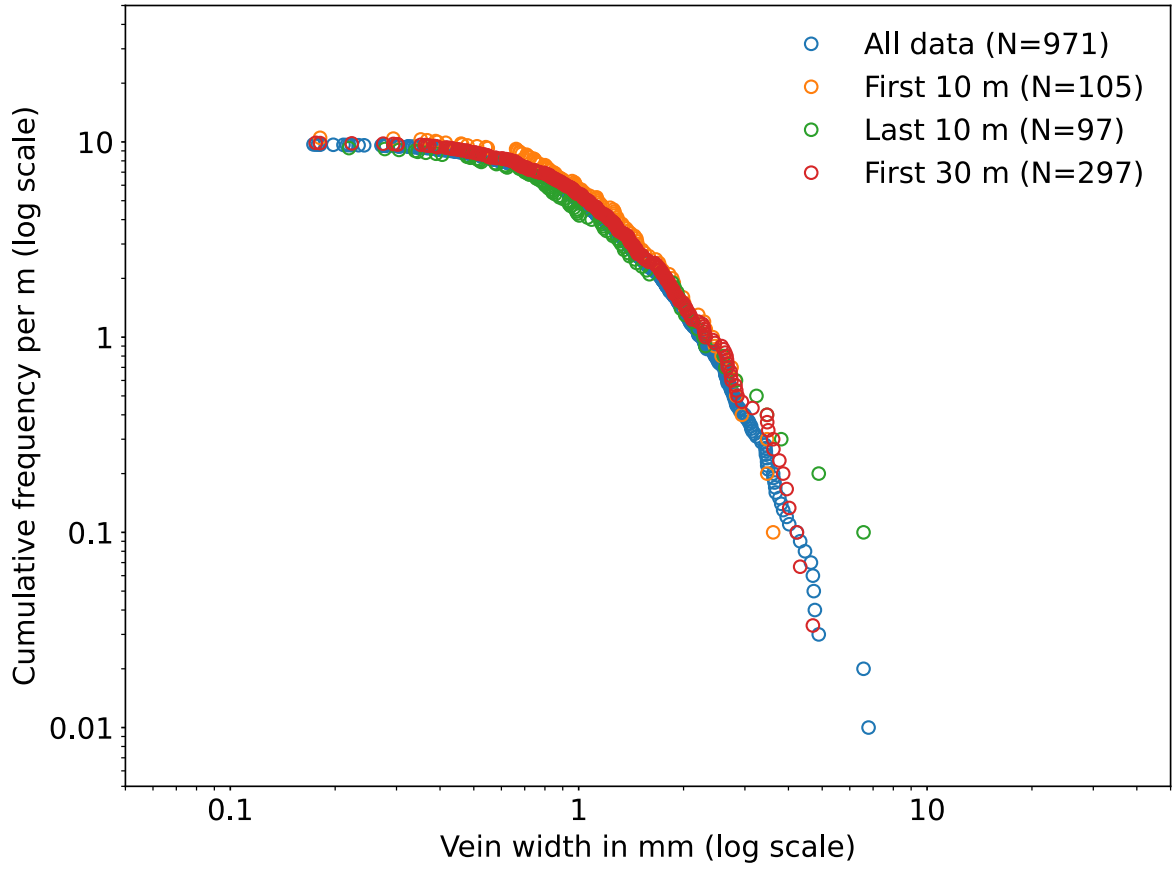

Figure 28. Cumulative frequency of vein widths along a 100 m scanline: Log-Log plot comparing full and localized samples

It was stated that fractures should show a power-law distribution, however in some cases they might not, and reasons are unclear. To understand this, vein data were syntetically generated along a 100-meter distance based on field observations: an average width of 1.0 mm (± 0.6 mm standard deviation), a minimum of 0.05 mm, and an average spacing of 0.1 m (± 0.075 m standard deviation), using Python. As a result, 971 veins were generated, and the cumulative frequency distribution of vein widths was plotted on a log-log scale. This was followed by retrieving data from the first and last 10 meters of the total distance, as well as from the first 30 meters (**Figure 28**). **Figure 28** demonstrates the risk of biased interpretation of the data when relying on smaller sampling distances, and particullary for wider width values. The variation in frequency distributions between localized samples (first and last 10 m) and the full 100 m might show spatial heterogeneity in vein development, possibly due to changes in local stress conditions, lithological variation, or fault-related structures. For structural analysis, especially when assessing fracture density longer and more continuous sampling is critical for capturing the true variability and distribution of veins.

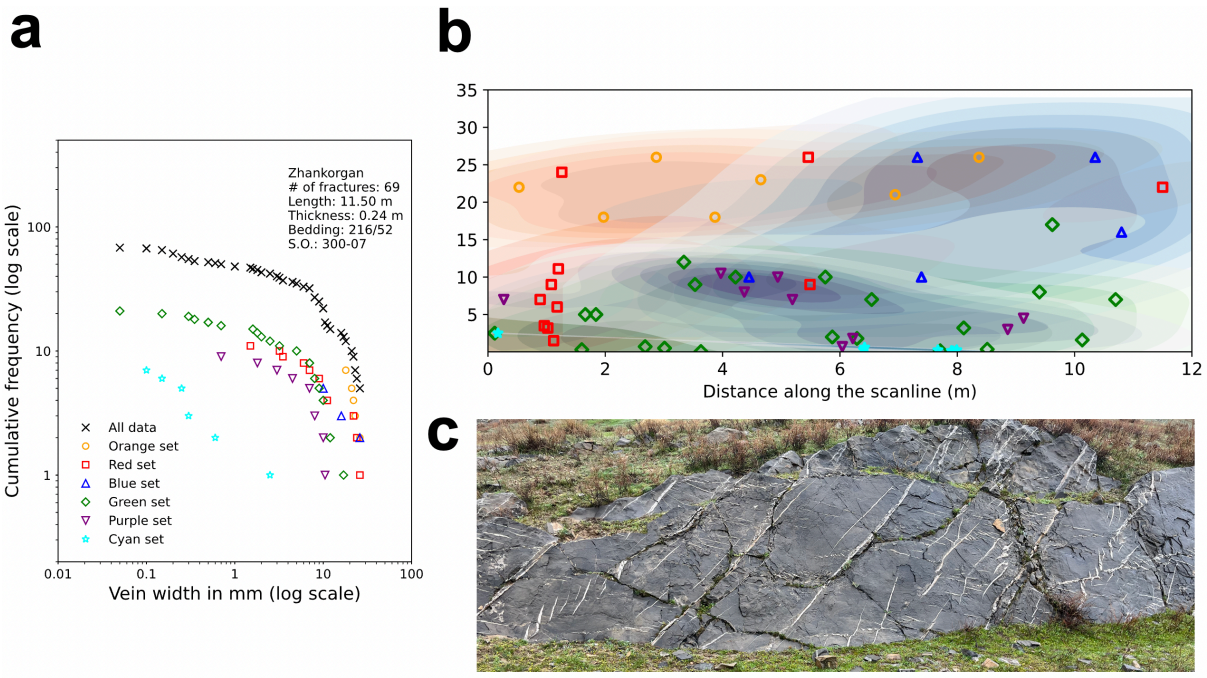

Figure 29. (a) Cumulative frequency of vein widths along the scanline in Zhankorgan section. (b) Distribution of vein widths along the scanline, and (c) a photo of the bed where scanline measurements were performed.

For instance, in the case of the Zhankorgan section, which is stratigraphically below the Akuyuk Reef Complex, the scanline length was approximately 12 m. Within this interval, several vein sets were identified based on field observations. As shown in **Figure 29b-c**, these vein sets exhibit preferred orientations and spacing. Some sets may only appear within specific intervals. All of this highlights the importance of using scanlines of at least 10 meters to capture

the broader structural pattern. Additionally, as illustrated in the **Figure 29a**, the trendline becomes smoother with an increasing number of measurements, as also demonstrated in the generated dataset.

4.4. The Influence of Bed Thickness on Fracture Intensity

The relationships between the number of veins per meter and sum of vein width per meter with bed thickness were examined and depicted separately in **Figure 30**. The results of this study indicate a very weak inverse relationship for grainstone (**Figure 30a**) in terms of the number of veins per meter, demonstrating that an increase in bed thickness corresponds with a slight decrease in the number of veins. However, for rudstone, no direct relationship was observed. The same applies to the sum of vein width per meter for both lithologies, where no direct correlation was identified (**Figure 30b**). Based on this, it can be suggested that the Dunham classification of rock types has a weak or even no influence on the correlation between fracture intensity and bed thickness within the Aktobe section. Therefore, the next step was to see the effect of the facies.

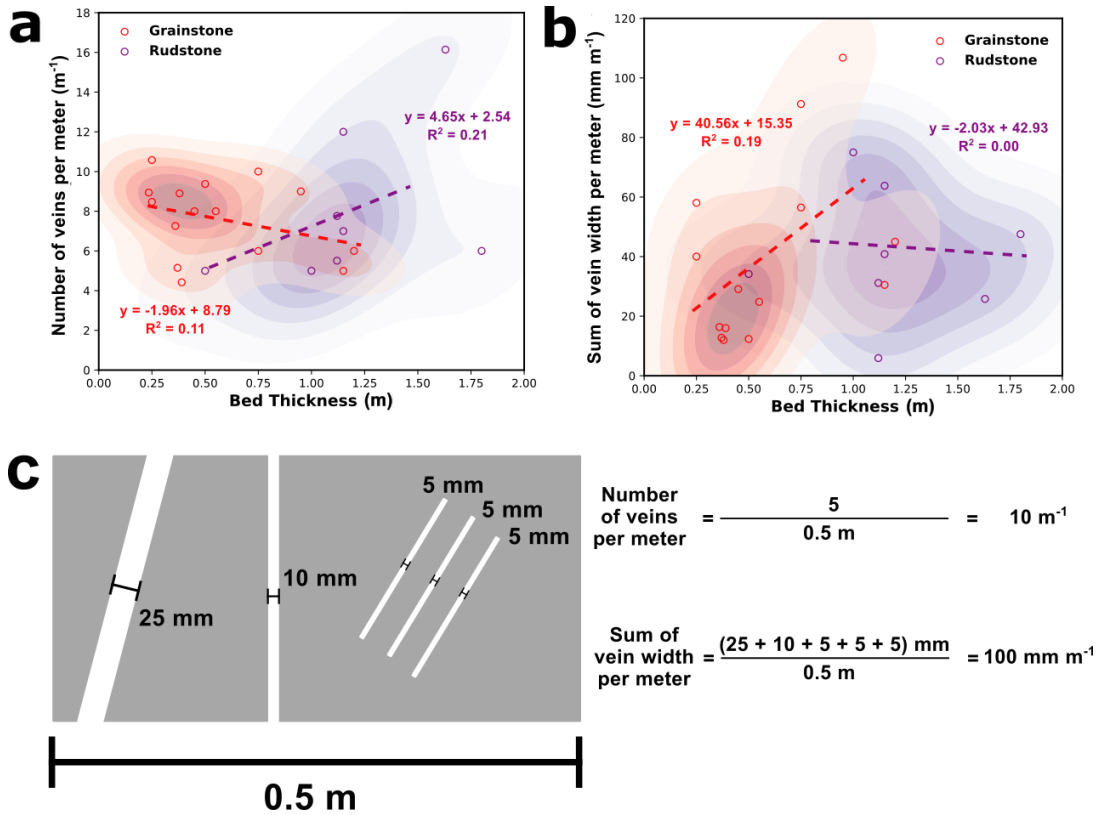

Figure 30. (a) The relationship between bed thickness and the number of veins per meter for grainstone (red) and rudstone (purple), with density contours illustrating data trends. (b) The sum of vein width per meter plotted against bed thickness. (c) A schematic diagram showing vein measurements and an example of the calculation process.

To observe the relationship between the number of veins and facies or depositional processes, the scanline results were tabulated based on number of veins per meter in ascending order (**Table 5**). The information about the facies present in the Aktobe section is demonstrated in **Appendix D**.

Although there is no distinct trend, some correlations might be identified. According to **Table 5**, at the mud-lean packstone facies, there are the fewest number of veins per meter. Despite mud-lean packstone has brittle nature, it might exhibit lower vein intensity due to several factors. To begin with, early diagenetic processes can lead to the precipitation of cements that bond grains together, increasing the rock's overall strength and reducing its tendency to fracture by occluding pore spaces and filling potential fracture initiation points (Lucia, 2007).

Table 5. Number of veins per meter for beds in ascending order with sedimentological characteristics (courtesy of Mynbayeva for providing data regarding facies and depositional processes for the given beds).

Bed #	Number of veins per meter [m^{-1}]	Sum of vein width per one meter [mm m^{-1}]	Rock Type	Thickness	Grainsize	Facies	Depositional Process
36	3	11.2	Grainy Wackstone	0.12	Medium	F7	
91	4.42	16.01	Grainy Wackstone	0.39	Fine	F7	
1	5	75	Rudstone	1	Medium	F3	Ta
2	5	34.15	Rudstone	0.5	Fine	F3	Ta
31	5	30.5	Grainstone	1.15	Very Coarse	F1	F1b
71	5.15	12.78	Grainstone	0.37	Coarse	F3	Ta
80	5.51	5.92	Rudstone	1.12	Pebble	F1	F1b
34	5.9	23.45	Muddy packstone	0.11	Fine	F3	Tb
3	6	56.5	Grainstone	0.75	Coarse	F1	F1b
4	6	45	Grainstone	1.2	Coarse	F2	F2b
20A	6	47.55	Rudstone	1.8	Granule	F5	GD
20B	7	63.8	Rudstone	1.15	Granule	F1	F1b
114	7.26	16.37	Grainstone	0.36	Coarse	F3	Ta
80	7.76	31.17	Rudstone	1.12	Pebble	F1	F1b
19	8	29.1	Grainstone	0.45	Coarse	F3	Ta
25	8	24.8	Grainstone	0.55	Coarse	F3	Tb
67	8.47	58.06	Grainstone	0.25	Medium	F3	Ta
69	8.9	11.99	Grainstone	0.38	Coarse	F3	Ta
43	8.94	56.72	Grainstone	0.235	Fine	F3	Ta
9	9	106.8	Grainstone	0.95	Very Coarse	F3	Ta

103	9.375	12.35	Grainstone	0.5	Medium	F3	Ta
8	10	91.25	Grainstone	0.75	Coarse	F3	Ta
15	10.58	40.02	Grainstone	0.25	Very Fine	F3	Ta
22	12	40.85	Rudstone	1.15	Granule	F1	F1b
13	16.14	25.8	Rudstone	1.63	Very Coarse	F3	Tb

Appindix C goes as supplementary for **Table 5** to describe facies in Aktobe section.

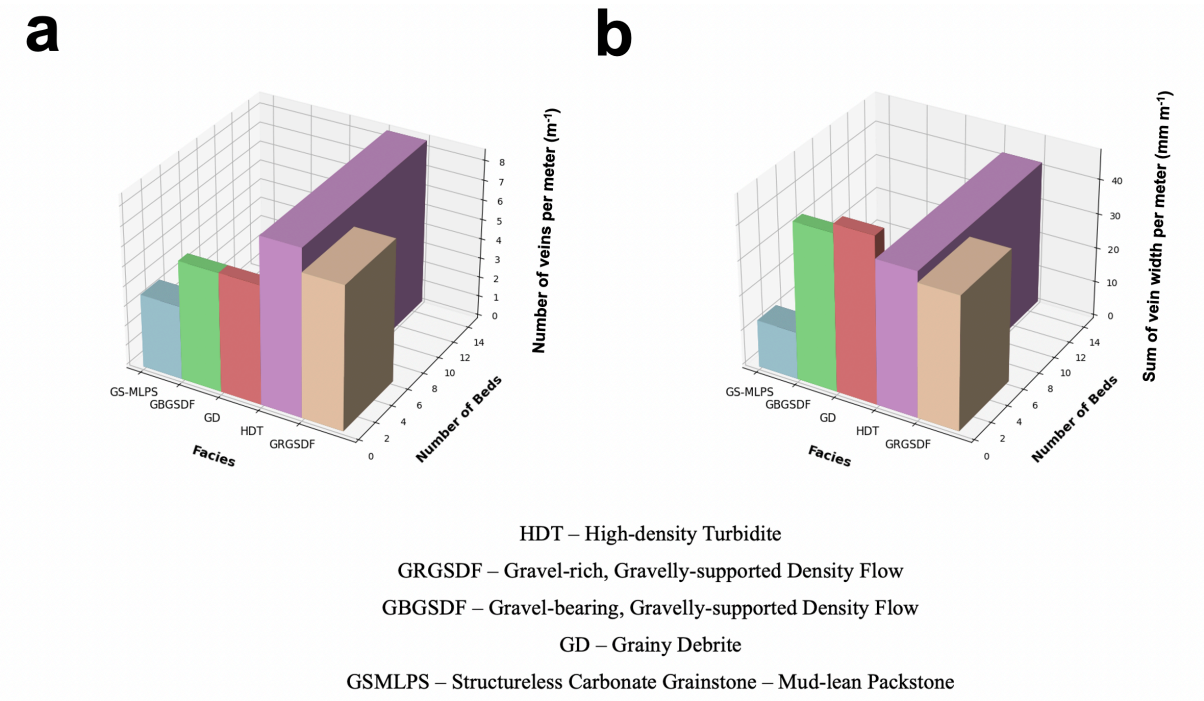

Figure 31. 3D bar plots showing vein characteristics across different sedimentary facies.: (a) number of veins per meter per facies and (b) sum of vein width per meter per facies.

Figure 31 shows 3D bar plots of the vein frequency and intensity across differnet sedimentary facies, along with the corresponding beds numbers. Based on the plots we might see that the gravel-rich, gravelly-supported density flows (GRGSDF) have the highest vein frequency and intensity, followed closely by high-density turbidites (HDT). This might suggest that the existence of a strong structural response to tectonic stress or compaction in more lithified and coarser grained deposits which are more prone to vein formation due to brittle deformation nature (Bons et al., 2012; Ramsay and Huber, 1983).

In comparison, structureless grainstone to mud lean packstone facies (GSMLPS) exhibit minimum vein development that can be interpreted as a devolopment of the more ductile

character of the rocks under stress or minimum permeability contrast which prevents fluid flow and vein precipitation (Laubach et al., 2004).The higher vein intensities in GRGSDF and HDT beds also indicate successful fluid flow and vein filling processes, likely caused by better fracture connectivity and higher original porosity in these facies. To visualize fracture network of the Aktobe section **Figure 33** was prepared based on the sedimentological log by Arnoud Sloutman which was modified using fracture data from the scanlines, along with observations from the outcrop. From **Figure 33** and **Table 5**, it can be observed that the vein intensity is higher in the upper fine-grained part (top of the bed) compared to the lower coarse-grained region (base of the bed), which contains crinoids, brachiopods, and some rugose corals. The same was seen in bed #3 were set 2 and 3 are mostly in fine-grained regions. Although, it was thought that with thin beds there used to be more fractures, at bed # 6 vein intensity is low. This might be due to the presence of the chert. The relation between facies type, bedding features, and vein distribution might confirm the interplay between mechanical stratigraphy and diagenetic alteration in controlling vein systems in sedimentary basins (Nelson, 2001). However, the differences are not significant, and more importantly, the corresponding number of beds is not sufficient to draw solid conclusions. Therefore, as a next step we need to refer to the stylolites.

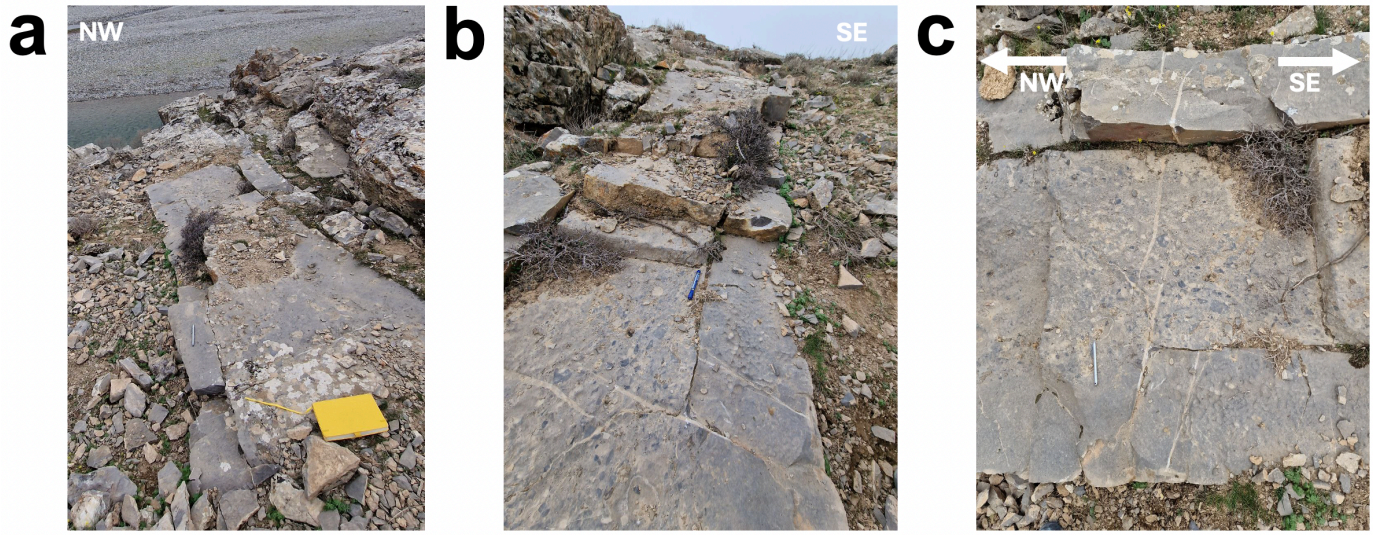

Figure 32. Bed 80 in the Aktobe section, viewed to the NW (a), SE (b) and from the side (c).

We can observe that at the beginning of Bed 80 (**Figure 32a**), there is only one bed, while further along it splits into two beds with a stylolite in between (**Figure 32b**). The stylolite terminates at the tension gash (set AT2), which indicates that the stylolite is younger than the tension gashes (**Figure 32b** and **c**). This kind of example can be seen not only in the Aktobe section but also clearly in the Akuyuk section.

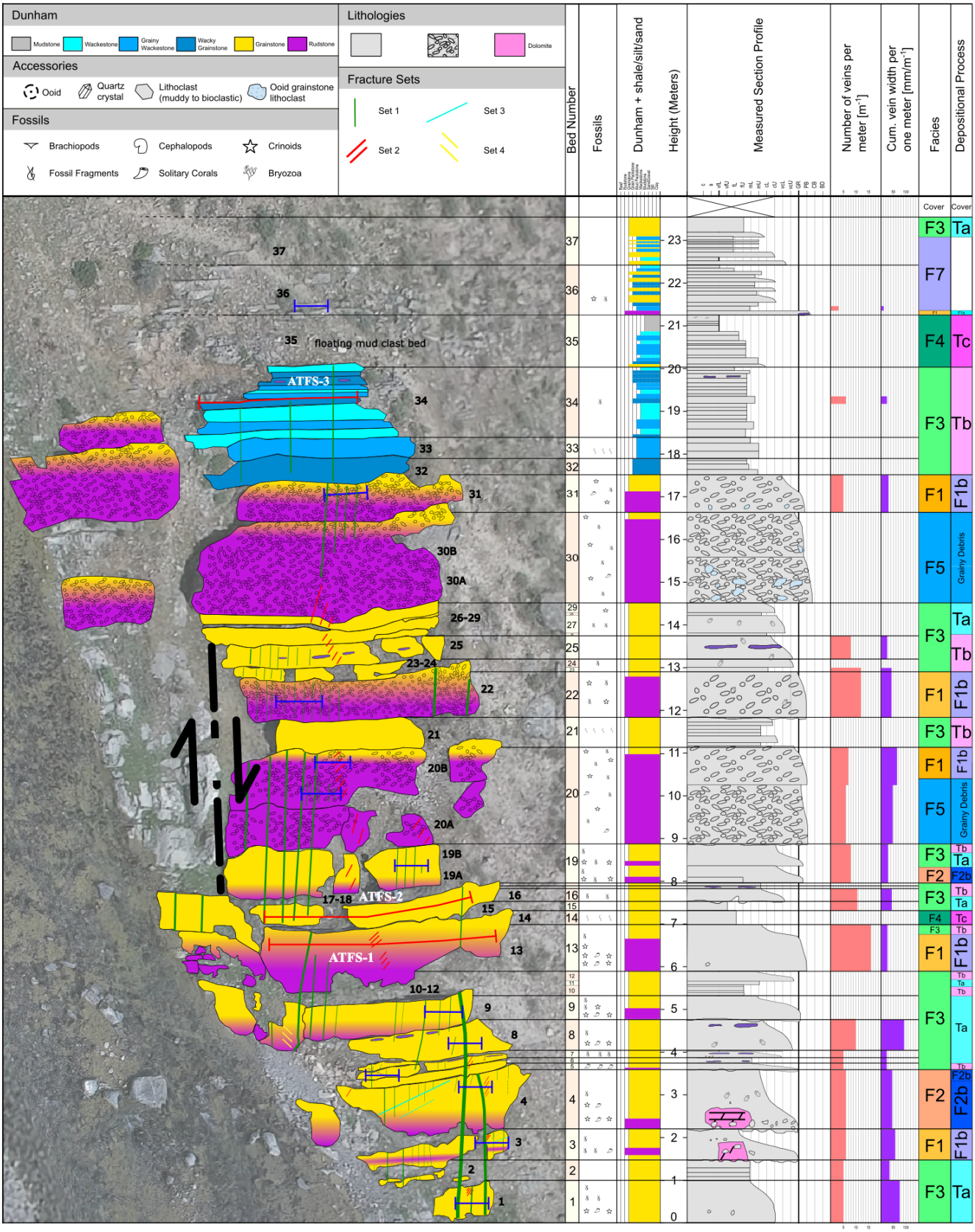

Figure 33. First 24 meters of the Aktobe section with a sedimentological log indicating bed number, Dunham classification, measured section profile, fracture intensity, cumulative fracture width, facies, and depositional processes with vein sets in map view.

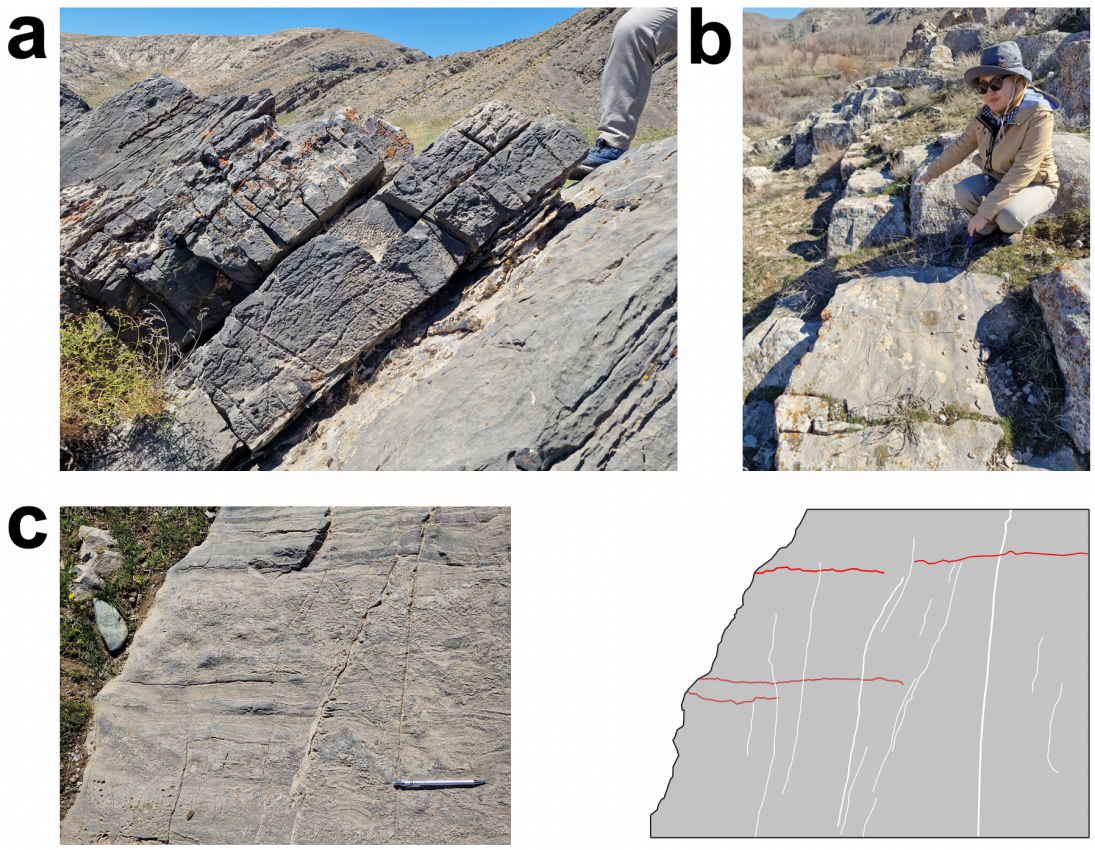

Figure 34. Transition of stylolites observed in (a) the main Akuyuk section and (b–c) the SW limb of the Akuyuk Syncline within the Famennian period intervals. A schematic illustration of photo (c) is shown to the right of the photo.

In **Figure 34a**, it is clearly visible how the bed just above the foot (upper part) consists of two "beds", while further below it appears as a single "bed". The boundary between them is a stylolite which terminates halfway. This phenomenon occurs throughout the main Akuyuk section. In the sedimentological log (**Figure 35**) which was prepared by Dinara Nadirkhanova and modified using fracture data from the scanlines, along with observations from the outcrop, we can see numerous cases where bed boundaries are actually stylolites. In some places, there are sedimentological and grain size differences between these "beds", while in others there are none. The same feature can be observed in the SW limb of the Akuyuk Syncline, where the same rocks are present. In the upper part of the **Figure 34b** two separate beds might be seen while in the lower part there is just one. The change in the lithology is not visible. As well as significant differences in grain sizes. In **Figure 34c**, on the middle-left side of the bed, there is a bedding parallel stylolite that has weathered into a small gully and disappears on the right side. Additionally, we can observe thin veins cutting through the stylolite, and as well as how the stylolite cuts through the veins.

Figure 35. The detailed measured section of the Akuyuk area showing the distribution of vein sets and the locations of stylolites along the sedimentological log.

Based on **Figure 35**, the bedding we see at the beginning gradually disappears and transitions into a stylolite oriented parallel to the original bedding planes at the end. Therefore, what appears to be bedding to observers is probably not true bedding at all but rather a weathered stylolite. In most cases, as seen in the Akuyuk section, misleading field observations occur due to an illusion of stratification that appears when erosion follows stylolitic surfaces. This phenomenon is particularly common in carbonate rocks, where acidic water interactions (meteoric rain) accelerate dissolution processes, carving out pseudo-bedded structures. The irregularity of stylolite surfaces may lead to an increase in resistance to fluid flow due to higher frictional forces, while relatively smoother fracture surfaces result in lower fluid transport rates. In turn, the rate at which stylolite dissolve influences stress distributions in the surrounding rock (localized pressure build-up), which can affect its overall strength, rate of deformation or the propagation of fractures. Most importantly, when it comes to fracture characterization, it is crucial to distinguish real bedding, as data collection may lead to incorrect assumptions. For instance, veins that appear to terminate at bedding planes may, in reality, be terminating at the stylolite. It also should be considered that the growth of stylolite might assist the opening of perpendicular veins, triggered by fluid over pressure along the interface.

5. CONCLUSIONS

The fractures (veins) in the carbonate platform of the Bolshoi Karatau mountains were studied because this platform has the same age and lithology as the carbonate platform of the Tengiz oil reservoir and is considered to be a well-exposed analogue. An important difference appeared to be, first, that the fractures occur as mineralised fractures, i.e. veins, notably calcite veins, and not as open fractures, such as in the Tengiz platform. Second, whereas fractures in the Tengiz carbonate platform are considered to be burial fractures, i.e. formed due to burial or during burial, or directly related to differential compaction and slope instability syn-sedimentary fractures, the veins in the Bolshoi Karatau carbonate platform primarily appear to be tectonic veins formed during the Hercynian orogeny formed during thrusting, faulting and folding of the rocks. Third, large parts of these veins are fibrous veins, believed to be formed as crack-seal veins, so the width of the veins as measured in the field is a cummulative width, representing the sum of numerous fracture events with an open fracture width many times smaller than the observed cummulative one. It can be concluded:

1. The veins are tectonic veins formed during the Hercynian orogeny
2. Statistical analysis of vein spacing, width, height and length can be summarised as follows: In the Aktobe section, the dominant vein set has an average width of 3.7 ± 1.0 mm, an average spacing of 0.2 ± 0.1 m, an average height of 0.3 ± 0.1 m and in beds of 1.0 ± 0.5 m thick. In the Akuyuk section the dominant vein set has an average vein width of 1.0 ± 0.6 mm, with an average spacing of 0.1 ± 0.02 m and an average height of 0.3 ± 0.1 m in beds of 0.2 ± 0.1 m thick. The calcite vein coverage, expressed as a percentage of the wall rock for the dominant set is 2.0 ± 0.7 % in the Aktobe section and 0.4 ± 0.1 % in the Akuyuk section.
3. Vein density showed no significant dependence on bed thickness and on the rock type as indicated by R^2 values of 0.11 for grainstone and 0.21 for rudstone.
4. Young's modulus of the grain stones and the rudstones derived from Schmidt hammer rebound values is 66 ± 12 GPa.
5. Vein width of dominant sets in cummulative log-log plots exhibited multi segmented power-law behavior, with segmented trendlines for both sections.
6. The change in slope in the curves may be due to insufficient length of the scanlines in question. These should be longer than 10 m.
7. In many cases, stylolites had replaced original bedding surfaces which created a misleading impression of stratification.

6. WHAT SHOULD WE DO NEXT?

Based on the current results, it is recommended to explore outcrops regardless of the abundance or deficiency of veining. Prior to conducting any measurements, stylolites should be carefully identified and examined, as confusion may arise as was observed in Akuyuk section. Beds selected for scanline measurements should also be chosen independent of the number of visible veins, considering that they are sufficiently exposed. Since performing scanline measurements can be time consuming, it is suggested to involve assistants who are introduced about the veins in advance, with clear measurement standards established for consistency. To ensure data reliability, the performance of individuals can be standardised by assigning the same scanline to multiple people and comparing results. Scanline lengths should ideally exceed 10 meters, but if that is not applicable, the available data can still provide valuable insights and may be applied appropriately. Finally, veins and wall rocks should be examined microscopically in thin section. Although the analysis was initiated, it was not completed, and therefore the results were not presented.

7. REFERENCES

Alexeiev, D. V., Cook, H.E., Buvtyshkin, V.M., Golub, L.Y., 2009. Structural evolution of the Ural–Tian Shan junction: A view from Karatau ridge, South Kazakhstan. Comptes Rendus. Géoscience 341, 287–297. https://doi.org/10.1016/j.crte.2008.12.004

Allen, M.B., Alsop, G.I., Zhemchuzhnikov, V.G., 2001. Dome and basin refolding and transpressive inversion along the Karatau Fault System, southern Kazakstan. J Geol Soc London 158, 83–95. https://doi.org/10.1144/jgs.158.1.83

Aydin, A., 2009. ISRM Suggested method for determination of the Schmidt hammer rebound hardness: Revised version. International Journal of Rock Mechanics and Mining Sciences. https://doi.org/10.1016/j.ijrmms.2008.01.020

Bai, T., Pollard, D.D., 2000. Fracture spacing in layered rocks: a new explanation based on the stress transition. J Struct Geol 22, 43–57. https://doi.org/10.1016/S0191-8141(99)00137-6

Belka, Z., Dopieralska, J., Jakubowicz, M., Skompski, S., Walczak, A., Korn, D., Siepak, M., 2021. Nd isotope record of ocean closure archived in limestones of the Devonian–Carboniferous carbonate platform, Greater Karatau, southern Kazakhstan. J Geol Soc London 178. https://doi.org/10.1144/jgs2020-077

Bogdanov, A.A., 1947. The intensity of cleavage as related to the thickness of beds (in Russian). Soviet Geology 16.

Bons, P.D., Elburg, M.A., Gomez-Rivas, E., 2012. A review of the formation of tectonic veins and their microstructures. J Struct Geol 43, 33–62. https://doi.org/10.1016/j.jsg.2012.07.005

Bourne, S.J., 2003. Contrast of elastic properties between rock layers as a mechanism for the initiation and orientation of tensile failure under uniform remote compression. J Geophys Res 108. https://doi.org/10.1029/2001jb001725

Burtman, V., 1964. Talaso-Fergana wrench fault (Tien-Shan). Geological Institute Academy of Sciences of the USSR, Moscow.

Butler, R.W.H., Tavarnelli, E., Grasso, M., 2006. Structural inheritance in mountain belts: An Alpine–Apennine perspective. J Struct Geol 28, 1893–1908. https://doi.org/10.1016/j.jsg.2006.09.006

Collins, J., Kenter, J.A.M., Harris, P.M., Kuanysheva, G., Fischer, D.J., Steffen, K.L., 2006. Facies and Reservoir-quality Variations in the Late Visean to Bashkirian

Outer Platform, Rim, and Flank of the Tengiz Buildup, Precaspian Basin, Kazakhstan, in: AAPG Memoir. American Association of Petroleum Geologists, pp. 55–95. https://doi.org/10.1306/1215874M881469

Collins, J., Narr, W., Harris, P.M., Playton, T., Jenkins, S., Tankersley, T., Kenter, J.A.M., 2013. Lithofacies, depositional environments, burial diagenesis, and dynamic field behavior in a carboniferous slope reservoir, tengiz field (republic of Kazakhstan), and comparison with outcropanalogs, in: SEPM Special Publications. SEPM Society for Sedimentary Geology, pp. 50–83. https://doi.org/10.2110/sepmsp.105.11

Cook, H.E., Zhemchuzhnikov, V.G., Zempolich, W.G., Zhaimina, V.Ya., Buvtyshkin, V.M., Kotova, E.A., Golub, L.Ya., Zorin, A.Ye., Lehmann, P.J., Alexeiev, D.V., Giovannelli, A., Viaggi, M., Fretwell, N., Lapointe, P., and Corboy, J.J., 2002. Devonian and Carboniferous carbonate platform facies in the Bolshoi Karatau, southern Kazakhstan: Outcrop analogs for coeval carbonate oil and gas fields in the North Caspian Basin, western Kazakhstan in: Paleozoic Carbonates of the Commonwealth of Independent States (CIS). SEPM (Society for Sedimentary Geology), pp. 81–122. https://doi.org/10.2110/pec.02.74.0081

Cook, H.E., ZHEMCHUZHNIKOV, V.G., ZEMPOLICH, W.G., ZHAIMINA, V.YA., BUVTYSHKIN, V.M., KOTOVA, E.A., GOLUB, L.YA., ZORIN, A.YE., LEHMANN, P.J., ALEXEIEV, D. V., GIOVANNELI, A., VIAGGI, M., FRETWELL, N., LAPOINTE, P., CORBOY, J.J., 2002. Devonian and Carboniferous Carbonate Platform Facies in the Bolshoi Karatau, Southern Kazakhstan: Outcrop Analogs for Coeval Carbonate Oil and Gas Fields in the North Caspian Basin, Western Kazakhstan, in: Paleozoic Carbonates of the Commonwealth of Independent States (CIS). SEPM (Society for Sedimentary Geology), pp. 81–122. https://doi.org/10.2110/pec.02.74.0081

Dong, L., Xu, H., Fan, P., Wu, Z., 2021. On the Experimental Determination of Poisson's Ratio for Intact Rocks and Its Variation as Deformation Develops. Advances in Civil Engineering 2021. https://doi.org/10.1155/2021/8843056

Friedman, M., 1972. Residual elastic strain in rocks. Tectonophysics 15, 297–330. https://doi.org/10.1016/0040-1951(72)90093-5

Fukunari, T., Gudmundsson, J.; A., Holloway, R., 2016. IPTC-18701-MS Model Fracture Formation in Mechanical Layers During Basin Burial Effects of Mechanical Properties Stress Fields Pore-Pressure and Layer Thickness.

Gross, M.R., Fischer, M.P., Engelder, T., Greenfield, R.J., 1995. Factors controlling joint spacing in interbedded sedimentary rocks: integrating numerical models with field observations from the Monterey Formation, USA. Geological Society, London, Special Publications 92, 215–233. https://doi.org/10.1144/GSL.SP.1995.092.01.12

Hobbs, D.W., 1967. The Formation of Tension Joints in Sedimentary Rocks: An Explanation. Geol Mag 104, 550–556. https://doi.org/10.1017/S0016756800050226

HOLDSWORTH, R.E., BUTLER, C.A., ROBERTS, A.M., 1997. The recognition of reactivation during continental deformation. J Geol Soc London 154, 73–78. https://doi.org/10.1144/gsjgs.154.1.0073

Holzhausen, G.R., Johnson, A.M., Burnham, C.W., Allen, C.R., Muehlberger, W., 1989. ORIGIN OF SHEET STRUCTURE, 1. MORPHOLOGY AND BOUNDARY CONDITIONS, Engineering Geology.

Huang, Q., Angelier, J., 1989. Fracture spacing and its relation to bed thickness. Geol Mag 126, 355–362. https://doi.org/10.1017/S0016756800006555

Ibrayev, F., Caspian, N., Company, O., Fermin Fernandez-Ibanez, ;, Degraff, J.M., 2016. SPE-182565-MS Using a Genetic-Based Approach to Enhance Natural Fracture Characterization in a Giant Carbonate Field.

Igizgali, A., 2024. Tectonic analysis of Aktobe and Zhankorgan valleys of the Bolshoi Karatau carbonate platform. Nazarbayev University.

Khamehchi, E., Khaleghi, M.R., Abbasi, A., Mahdavi Kalatehno, J., 2024. Estimating the Formation Fracture Pressure Through Geomechanical Modeling. pp. 45–73. https://doi.org/10.1007/978-3-031-58281-3_2

Ladeira, F.L., Price, N.J., 1981. Relationship between fracture spacing and bed thickness. J Struct Geol 3, 179–183. https://doi.org/10.1016/0191-8141(81)90013-4

Lake, L., 2007. Petroleum Engineering Handbook. Society of Petroleum Engineers, TX. https://doi.org/10.1016/j.egypro.2017.03.1713

Laubach, S.E., Olson, J.E., Gale, J.F.W., 2004. Are open fractures necessarily aligned with maximum horizontal stress? Earth Planet Sci Lett 222, 191–195. https://doi.org/10.1016/j.epsl.2004.02.019

Lisovsky, N., Gogonenkov, G., Petzoukha, Y., 1992. The Tengiz Oil Field in the Pre-Caspian Basin of Kazakhstan (Former USSR)-Supergiant of the 1980s, in: Giant

Oil and Gas Fields of the Decade 1978-1988. American Association of Petroleum Geologists, pp. 101–122. https://doi.org/10.1306/M54555C7

McQuillan, H., 1973. Small-Scale Fracture Density in Asmari Formation of Southwest Iran and its Relation to Bed Thickness and Structural Setting. Am Assoc Pet Geol Bull 57. https://doi.org/10.1306/83D9131C-16C7-11D7-8645000102C1865D

Narr, W., Flodin, E., 2012. Fractures in Steep-rimmed Carbonate Platforms: Comparison of Tengiz Reservoir, Kazakhstan, and Outcrops in Canning Basin, NW Australia*. AAPG Annual Convention and Exhibition, California.

Narr, W., Flodin, E.A., Playton, T.E., Heesakkers, V., 2024. Depositional and lithological control on fractures in a steep, reefal carbonate margin: Lennard Shelf outcrops of the Canning Basin, Western Australia. Am Assoc Pet Geol Bull 108, 1443–1484. https://doi.org/10.1306/02132423039

Narr, W., Suppe, J., 1994a. Kinematics of basement-involved compressive structures. Am J Sci 294, 802–860. https://doi.org/10.2475/ajs.294.7.802

Narr, W., Suppe, J., 1994b. Kinematics of basement-involved compressive structures. Am J Sci 294, 802–860. https://doi.org/10.2475/ajs.294.7.802

Nelson, R.A., 2001. Geologic Analysis of Naturally Fractured Reservoirs, 2nd ed. Gulf Professional Publishing.

Passchier, M., Passchier, C.W., Weismüller, C., Urai, J.L., 2021. The joint sets on the Lilstock Benches, UK. Observations based on mapping a full resolution UAV-based image. J Struct Geol 147. https://doi.org/10.1016/j.jsg.2021.104332

Ramsay, J.G., Huber, M.I., 1983. The Techniques of Modern Structural Geology. Academic Press.

Sachpazis, C.I., 1990. Correlating Schmidt hardness with compressive strength and Young's modulus of carbonate rocks. Bulletin of Engineering Geology and the Environment 42.1.

Sanderson, D.J., Peacock, D.C.P., Nixon, C.W., 2024. Fracture sets and sequencing. Earth Sci Rev. https://doi.org/10.1016/j.earscirev.2024.104888

Savage, W.Z., 1978. The development of residual stress in cooling rock bodies. Geophys Res Lett 5, 633–636. https://doi.org/10.1029/GL005i008p00633

Singh, T.N., Kainthola, A., Venkatesh, A., 2012. Correlation between point load index and uniaxial compressive strength for different rock types. Rock Mech Rock Eng 45, 259–264. https://doi.org/10.1007/s00603-011-0192-z

Tengizchevroil, 2023. Corporate responsibility report 2019- 2020.

Tsiambaos, G., Sabatakakis, N., 2004. Considerations on strength of intact sedimentary rocks. Eng Geol 72, 261–273. https://doi.org/10.1016/j.enggeo.2003.10.001

Umralin, A., Nadirkhanova, D., Bekeshov, D., Mynbayeva, T., 2024. Outcrop gamma-ray spectrometry as a tool for refining depositional environment and diagenetic history in Carboniferous carbonate slope deposits, Bolshoi Karatau, Kazakhstan. IAS International Meeting of Sedimentology.

Weber, L.J., Francis, B.P., Harris, P.M. (Mitch), Clark, M., 2003. Stratigraphy, Lithofacies, and Reservoir Distribution, Tengiz Field, Kazakhstan, in: Permo-Carboniferous Carbonate Platforms and Reefs. SEPM Society for Sedimentary Geology, Tulsa, Oklahoma, pp. 351–394. https://doi.org/10.2110/pec.03.78.0351

Zhaimina, V., Mustapaeva, S., Baybatsha, A., Belka, Z., 2014. The Viséan-Serpukhovian boundary in the Big Karatau Mountains (South Kazakhstan). Newsletter on Carboniferous Stratigraphy.

8. APPENDICES

Appendix A. Scanline sheets used for measurements

Section:

Scanline name:

People:

1.
2.

Date (dd/mm/yyyy):

GPS Coordinates:

Use Decimal degrees (DD): xx.xxxxx (at least 5 digits after the dot)

	Latitude	Longitude
Start point		
End point		

Sample(s): **Overview photo(s):**

Length of the Scanline [m]: ____

Make sure that there are at least 2 digits.

Thickness of the bed:

Measure thickness in cm at the starting, middle, and end points.

	Thickness [cm]
Start	
Middle	
End	

Thickness of the beds:

Measure thickness of the beds above and below the bed where the scanline was placed, in cm.

Second bed above	First bed above	Second bed below	First bed below

Bedding Orientation

Measure dip azimuth and dipping angle at the starting, middle, and end points.

	Orientation
Start	/
Middle	/
End	/

Scanline Orientation

Measure trend and plunge at the starting, middle, and end points.

#	Orientation
Start	-
Middle	-
End	-

Scanline Plane Orientation

Measure dip azimuth and dipping angle at various positions as need.

Position [m]	Orientation	Comments
	/	
	/	
	/	
	/	
	/	

References:

Layer in the Sedimentological Log	
Grain size	
Facies	

*Ensure that copies of the scanlines, along with photos, are provided to the responsible person. If you are unsure whom to send them to, please send them to **dias.bekeshov@nu.edu.kz**.*

Scanline Sheet ___ out ___

Fracture #	Position (m)	Fracture Set	Fracture (F) or Cluster C	# of Fractures in cluster	Dip azimuth	Dip angle	Fracture type	Max aperture (mm)	Fracture shape	Height upper (m)	Height lower (m)	Upper terminous	Lower terminous	Length side 1 (m)	Length side 2 (m)	Side 1 terminous	Side 2 terminous	Photo	Notes

Terminations	Fracture type	Shape
B=Bed	E=Extension	P = planar
F=Fracture	S=Shear	C = curved
S=Stylo	N=normal	I=irregular
O=Tips Out	R=Reverse	
C=Cover	SS=StrikeSlip	
Ch=Chert		

Scanline Sheet ___ out ___

You may use this page for sketches.

Scanline Sheet ___ out ___

Appendix B. Cumulative vein width distribution separately for each scanline in Aktobe section.

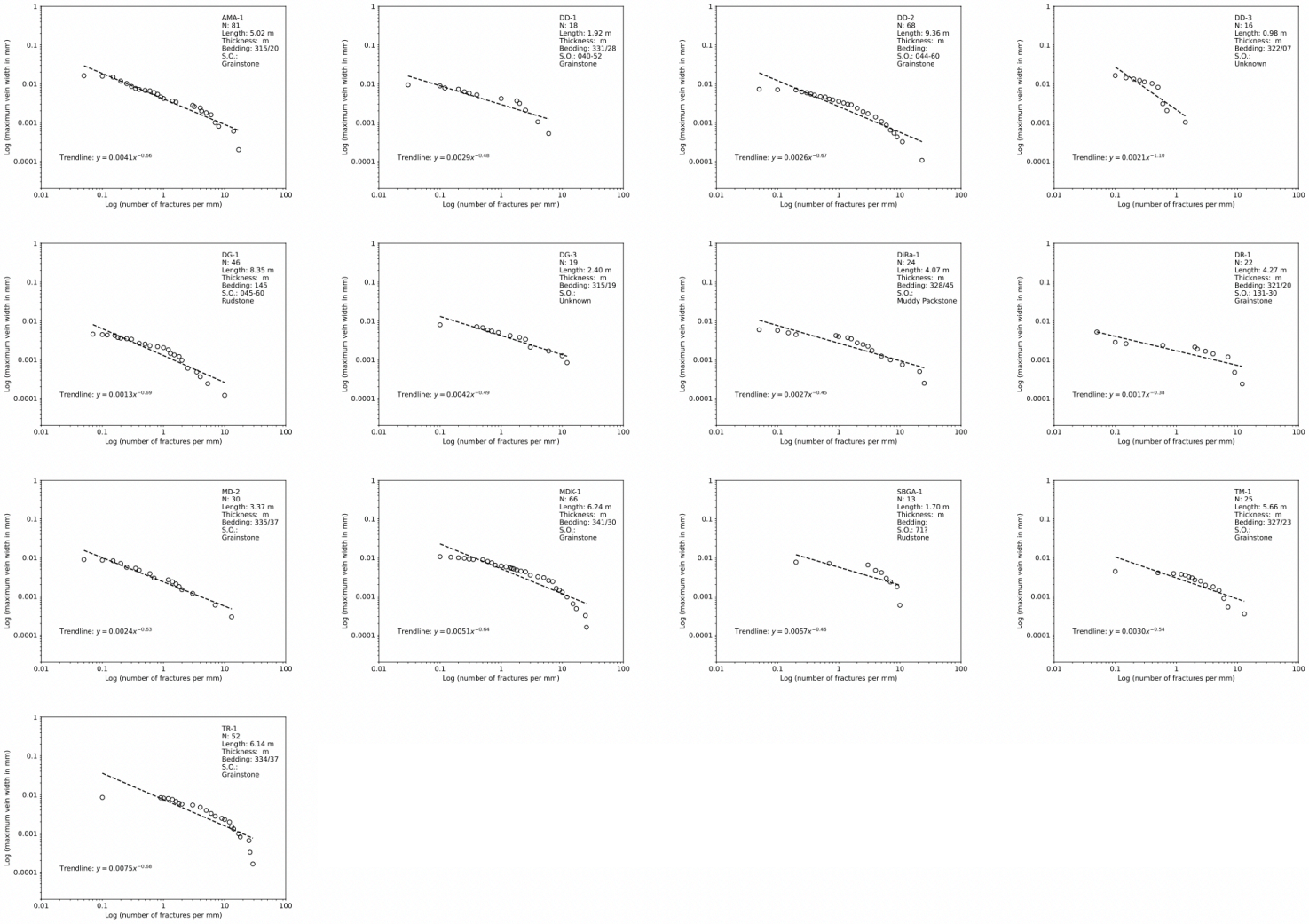

Appendix C. Cumulative vein width distribution separately for each scanline in Akuyuk section.

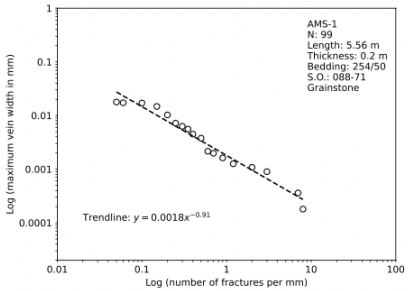

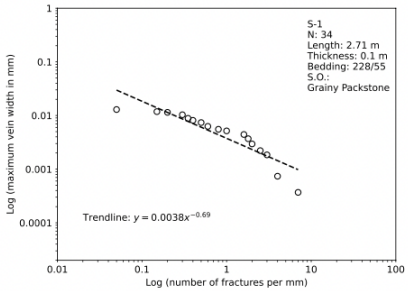

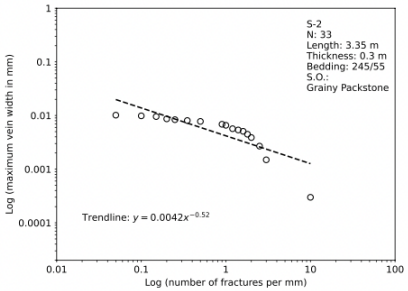

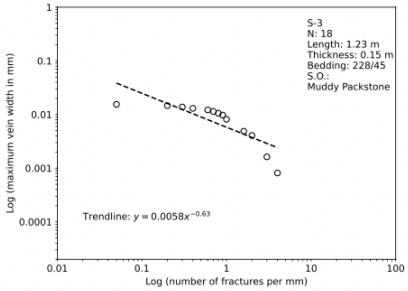

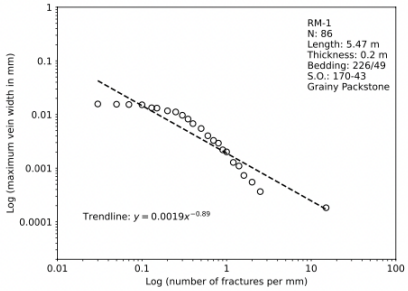

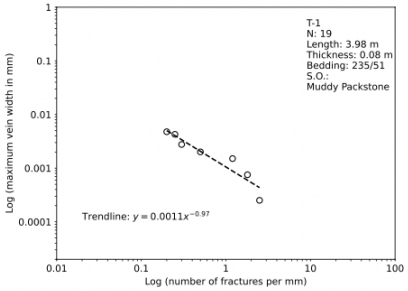

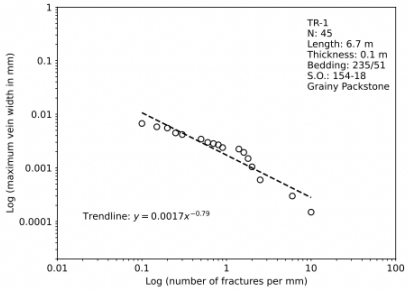

Appendix D. Information about the facies present in Aktobe section.

Facies number	Facies name	Description
F1	Gravel-rich Gravelly-supported Density Flow	Massive texture; Commonly normally graded , but can exhibit inverse grading as well; >30% gravel with coarse to very coarse sand.
F2	Gravel-bearing Gravelly-supported Density Flow	Massive texture; Commonly normally graded , but can exhibit inverse grading as well; 5-30% gravel with coarse to very coarse sand.
F3	High-density Turbidite (Ta-Tb)	Ta – Massive to normally graded grainstone – mud-lean packstone (locally floatstone or rudstone); Result of high-concentration suspension fall-out. Tb – Planar-laminated grainstone and mud-lean packstone; Result of upper flow regime.
F4	Low-density Turbidite (Tc-Te)	Tc – Current rippled mud-rich packstone, mud-lean packstone, grainstone; Result of lower flow regime. Td – Planar-laminated mudstone, wackestone, mud-rich packstone; Result of lower flow regime. Te – Laminated to massive mudstone and wackestone; Result of low-concentration suspension fall-out.
F5	Grainy Debrite	Grain and/or clast-supported; Disorganized 'floating' clasts; Massive texture; May exhibit weak vertical grading.
F6	Muddy Debrite	Matrix-supported; Disorganized 'floating' clasts and grains; Mudstone-Wackestone matrix; Massive texture; May exhibit weak vertical grading.
F7	Structureless carbonate Grainstone – Mud-lean packstone (GS-MLPS)	Structureless grainstone and/or mud -lean packstone.
F8	Structureless carbonate Wackestone – Mud-rich packstone (WS-MRPS)	Structureless wackestone and/or mud -rich packstone.
F9	Chert	Continuous several cm's thick layer of silica.